Magnonic Crystals

Pawel Gruszecki and Maciej Krawczyk

Faculty of Physics, Adam Mickiewicz University in Poznan,

Umultowska 85, Poznań, 61-614 Poland

(Dated: September 26, 2015)

The Author version of the paper .

Final version published in:
J. Webster (ed.), Wiley Encyclopedia of Electrical and Electronics Engineering.
DOI: 10.1002/047134608X.W8295

I. INTRODUCTION

Spin waves (SWs), quantized as magnons, are coherent disturbances of magnetization in a magnetic medium, and can propagate in the form of waves over a distance of up to a few centimeters. Their frequency spans the range from hundreds of MHz to a few THz, with the respective wavelengths ranging from micrometers to nanometers, depending on the magnetic properties of the material, the experimental geometry and the magnitude of the applied magnetic field. Thus, within these time and space limits SWs can be used for transferring energy or transmitting and processing information. Moreover, the magnetization dynamics can be influenced by many external factors, such as magnetic field, electric current, spin current, electromagnetic field, elastic waves, strain, voltage or temperature gradient, all of which can be used for exciting SWs or controlling their propagation. Also, physical quantities related to these factors can be studied with the use of SWs. Thus, various technological applications can benefit from using SWs; this justifies the effort taken in recent years to study the SW dynamics and to design prototypes of spin wave-based devices or elements to complement existing technologies.

Material structuring is one of the major factors used for controlling the propagation of waves with short wavelengths in solids, especially when integration and miniaturization are required. The use of periodic structuring for controlling the wave dynamics has increased significantly since the discovery of photonic crystals in 1987,[1,2] though the effect of periodic modulation on the wave transmission was studied already at the end of 19th century. The effect of one-dimensional periodicity on vibration waves was considered at that time,[3] and a theory of differential equations with coefficients being periodic functions of an independent variable was developed by Floquet and Hill.[4,5] However, the extension of this theory to three dimensions and its application to electronic waves remain a vital step in solid state physics. A theory of electrons in a crystal lattice was developed in the 1920s, and the most important theorem for the description of waves in periodic media – Bloch's theorem – was established.[6] It is noteworthy that F. Bloch was also the first to develop a theory of spin waves.[7,8] On these theoretical grounds the concept of electronic passbands and stopbands (band gaps) was formulated to describe the conduction properties of semiconductors; these very properties provided a basis for the development of modern microelectronics. The usefulness of periodic structuring was verified in the following years, leading to the development of var-

ious kinds of resonators, filters, splitters and other devices for electromagnetic, mechanical or transmission lines.[9–11] Since 1987 periodicity has been extensively used for molding the flow of electromagnetic waves in the range from microwave to optical wavelengths, which led to the discovery of new materials with properties unheard of in nature. Concepts developed in photonics were transferred to other types of excitations, such as phonons, plasmons and magnons.

Already in the late 1970s periodicity was used for controlling SW excitations in ferromagnetic materials.[12,13] The transmission of magnetostatic waves was molded by periodic distribution of the saturation magnetization, realized by ion implantation,[14] a regular lattice of etched grooves in a magnetic dielectric, periodic modulation by metallic stripes or dots on top of a ferromagnetic film,[15,16] or periodic perturbation of the effective magnetic field. Due to limitations in fabrication and technology the investigations were limited to relatively large structures, in which the dipolar interaction prevailed over the exchange interaction. The discovery of photonic crystals renewed the interest in magnetic periodic structures, inspiring many new ideas, providing abundant new physics, and pushing magnetization dynamics studies in unexplored directions. The concept of **magnonic crystals** (MCs) was proposed as a SW counterpart of photonic crystals.[17–20] Thus, MCs can be regarded as magnetic materials with periodic distribution of the constituent materials or periodic modulation of some magnetic parameters (e.g. saturation magnetization or magnetocrystalline anisotropy), or other parameters relevant to the propagation of SWs, such as external magnetic field, film thickness, stress or a surrounding of the homogeneous ferromagnetic film.

In any periodic medium the eigensolutions of the wave equation in the linear regime fulfill Bloch's theorem and, regardless of the type of excitation, form a band structure in the frequency–wave vector space. Thus, the qualitative understanding of the formation of the magnonic (i.e., spin-wave) band structure can be based on classical textbooks of solid state physics and the solution of the scalar Schrödinger equation in a periodic potential[21] or the wave equation for the propagation of electromagnetic waves.[22] Nevertheless, the details of the band structure can only be derived from numerical calculations. Usually the magnonic band structure is studied in terms of its sensitivity to the geometry of the MC, material parameters or external fields. Moreover, SWs have a complex dispersion relation even in homogeneous thin films. The dispersion depends on the direction and magnitude of the wave vector, the proportion of the short-range exchange interaction to the long-range dipolar in-

teraction, the external shape of the sample, the magnitude of the applied static magnetic field, its orientation with respect to the direction of propagation, and the magnetocrystalline anisotropy. This means that the SW band structure of MCs will be influenced by many additional factors apart from those they have in common with other types of artificial crystals. This makes MCs an intriguing topic for scientific studies and the main subject of research in the field of **magnonics**.[23]

II. SPIN WAVES IN HOMOGENEOUS MEDIA

Basic in magnonics, the Landau-Lifshitz (LL) equation describes the time (t) and position ($\mathbf{r}$) dependence of the magnetization vector $\mathbf{M}(\mathbf{r},t)$:

$$\begin{aligned}\frac{d\mathbf{M}(\mathbf{r},t)}{dt} &= \gamma\mu_0\left[\mathbf{M}(\mathbf{r},t)\times\mathbf{H}_{\text{eff}}(\mathbf{r},t)\right]\\ &+ \frac{\alpha}{M_{\text{S}}}\left[\mathbf{M}(\mathbf{r},t)\times\frac{d\mathbf{M}(\mathbf{r},t)}{dt}\right],\end{aligned} \tag{1}$$

where γ and μ_0 are the gyromagnetic ratio and the permeability of vacuum, respectively (here we assume $\gamma = 176$ rad GHz/T and $\mu_0 = 4\pi\times10^{-7}$ m T/A); M_{S} is the saturation magnetization, and $\mathbf{H}_{\text{eff}}(\mathbf{r},t)$ denotes the effective magnetic field. The last term in Eq. (1) describes energy dissipation, with α being a dimensionless damping parameter. The right side of the equation can be supplemented with additional terms related to other factors, e.g., spin-torque currents.

A small disturbances of magnetization from its equilibrium orientation, usually can be considered in the linear approximation; this means that in a ferromagnetic material saturated along the z-axis the magnetization vector can be split into static and dynamic parts, $\mathbf{M}(\mathbf{r},t) = M_z\hat{z}+\mathbf{m}(\mathbf{r},t)$, and all terms nonlinear with respect to the dynamic magnetization $\mathbf{m}(\mathbf{r},t)$ can be neglected in the equation of motion. Since $|\mathbf{m}(\mathbf{r},t)| \ll M_z$, we can also assume $M_z \approx M_{\text{S}}$, where M_{S} is the saturation magnetization. Here we will only consider monochromatic SWs; thus, for an angular frequency ω we can write $\mathbf{m}(\mathbf{r},t) = \mathbf{m}(\mathbf{r})\exp(i\omega t)$. Under these assumptions the dynamics of the magnetization vector $\mathbf{m}(\mathbf{r})$ with negligible damping is described by the stationary LL equation:

$$i\omega\mathbf{m}(\mathbf{r}) = \gamma\mu_0\left[M_{\text{S}}\hat{z}+\mathbf{m}(\mathbf{r})\right]\times\mathbf{H}_{\text{eff}}(\mathbf{r}). \tag{2}$$

In general the effective magnetic field can include a variety of components, depending on the material, structure and experimental conditions. Besides the exchange field, the

demagnetization field, the magnetocrystalline field or magnetostrictive components, it can also include components external to the ferromagnetic medium: external bias magnetic field or radio-frequency field. In one of relatively simple cases the considered effective magnetic field consists of the external magnetic field H_0, the dynamic magnetic field $\mathbf{h}^{\mathrm{ms}}$ created by the magnetization in precession, and the exchange field $\mathbf{h}_{\mathrm{ex}}$:

$$\mathbf{H}_{\mathrm{eff}}(\mathbf{r}) = H_0\hat{z} + \mathbf{h}^{\mathrm{ms}}(\mathbf{r}) + \mathbf{h}_{\mathrm{ex}}(\mathbf{r}). \tag{3}$$

The exchange field is related to the short-range interaction (usually limited to the nearest or next-nearest neighbors in the atomic crystal lattice), the energy of which is described by the Heisenberg Hamiltonian. However, in the linear approximation the exchange field can be defined as a differential operator of $\mathbf{m}$:

$$\mathbf{h}_{\mathrm{ex}}(\mathbf{r}) = l_{\mathrm{ex}}^2\nabla^2\mathbf{m}(\mathbf{r}), \tag{4}$$

where

$$l_{\mathrm{ex}} \equiv \sqrt{\frac{2A}{\mu_0 M_{\mathrm{S}}^2}} \tag{5}$$

is the exchange length and A is the exchange constant expressed in the units of J/m.

The dispersion relation of SWs in a homogeneous medium and Bloch's theorem are enough to elucidate the basic properties of the magnonic band structure. Even this, however, is not a straightforward task, since the SW dispersion relation depends on the shape of the magnetic body and is in general anisotropic. Here we will only discuss two cases: i) an isotropic homogenous ferromagnetic body, and ii) a homogeneous ferromagnetic thin film saturated with an in-plane or out-of-plane external magnetic field. The obtained information will provide a basis for the description of the SW dynamics in three-dimensional (3D) MCs and in MCs based on thin films periodic in one or two dimensions.

In a homogeneous body, shown in Fig. 1(a), the internal magnetic field is homogeneous, if we neglect the external shape effects (this theoretical model can be extended also to a body of ellipsoidal shape, but in that case the effective magnetic field from Eq. (3) needs to be supplemented with the homogeneous demagnetizing field).[24,25] Taking into account of Eq. (3), from Eq. (2) we can define the susceptibility tensor $\hat{\chi}$ [$\mathbf{m}(\mathbf{r}) = \hat{\chi}\mathbf{h}^{\mathrm{ms}}(\mathbf{r})$] and the

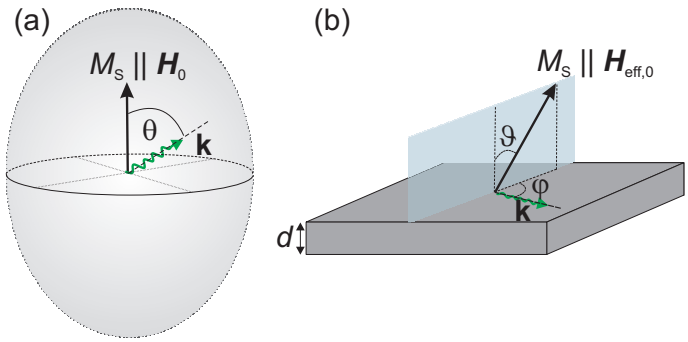

FIG. 1: Geometry used in the calculation of the spin wave (SW) dispersion relation in (a) a homogeneous ferromagnetic body (which can be of ellipsoidal shape, but with dimensions much larger than the SW wavelength), and (b) a thin film saturated by an external magnetic field H_0.

permeability tensor $\hat{\mu} \equiv \hat{1} + \hat{\chi}$ (where $\hat{1}$ is a unity matrix), the latter having the form:

$$\hat{\mu}_r = \begin{pmatrix} \mu^{xx} & i\mu^{xy} & 0 \\ -i\mu^{yx} & \mu^{yy} & 0 \\ 0 & 0 & 1 \end{pmatrix}, \tag{6}$$

where formally we write:

$$\mu^{xx} = 1 + \frac{\gamma^2 \mu_0^2 M_S (H_0 - M_S l_{ex}^2 \nabla^2)}{[\gamma\mu_0 (H_0 - M_S l_{ex}^2 \nabla^2)]^2 - \omega^2}, \tag{7}$$

$$\mu^{xy} = \frac{\gamma\mu_0 M_S \omega}{[\gamma\mu_0 (H_0 - M_S l_{ex}^2 \nabla^2)]^2 - \omega^2}, \tag{8}$$

$$\mu^{yx} = \mu^{xy}, \quad \mu^{yy} = \mu^{xx}. \tag{9}$$

The dynamic magnetic field is described by full Maxwell equations. However, in case of SWs of micrometer or shorter wavelength, considered for most applications in magnonics, the wavelength is much smaller than that of electromagnetic waves of the same frequency (e.g., 3 GHz electromagnetic radiation has a wavelength of 10 cm in air). This allows to use the magnetostatic approximation, in which Maxwell's equations reduce to:[26]

$$\begin{aligned} \nabla \times \mathbf{h}^{\mathrm{ms}}(\mathbf{r}) &= 0, \\ \nabla \cdot [\hat{\mu} \cdot \mathbf{h}^{\mathrm{ms}}(\mathbf{r})] &= 0. \end{aligned} \tag{10}$$

If we assume $\mathbf{h}^{\mathrm{ms}} = -\nabla\psi$, the first equation will become an identity for any analytical function ψ, and the scalar magnetostatic potential ψ will fulfill the Walker equation obtained directly from the second Eq. (10):[27]

$$\nabla \cdot (\hat{\mu} \cdot \nabla\psi) = 0. \tag{11}$$

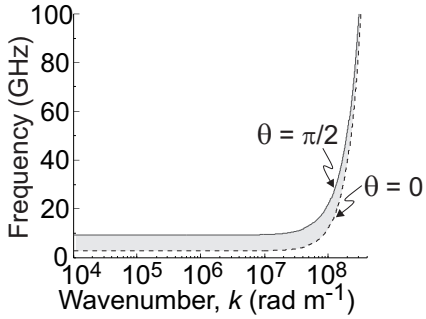

FIG. 2: The dispersion relation of SWs in a homogeneous material; dashed and solid lines refer to SW propagation parallel ($\theta = 0$) or perpendicular ($\theta = \pi/2$), respectively, to the external magnetic field. The dark area between these dispersions represents a SW manifold. The parameters of Py (reported in Table I) and 0.1 T external magnetic field were assumed in the calculations. The wavenumber axis has a logarithmic scale.

Assuming a plane-wave solution with a wave vector $\mathbf{k}$, $\psi \propto \exp(i\mathbf{k}\cdot\mathbf{r})$, and a SW propagation angle θ with respect of the direction of the bias magnetic field (which implies $k_x^2 + k_y^2 = k^2 \sin^2\theta$ and $k_z^2 = k^2\cos^2\theta$, Fig. 1(a)), the solution of Eq. (11) with the permeability tensor Eq. (6) is:[26,28]

$$\begin{aligned} \omega \;&=\; \gamma\mu_0 \left[(H_0 + M_{\rm S} l_{\rm ex}^2 k^2)\right. \\ &\times\; \left.(H_0 + M_{\rm S} l_{\rm ex}^2 k^2 + M_{\rm S}\sin^2\theta)\right]^{1/2}. \end{aligned} \tag{12}$$

This dependence of the SW frequency ($f = \omega/2\pi$) on the wave vector magnitude (the wavenumber k) is plotted in Fig. 2 for homogeneously magnetized permalloy in a magnetic field $\mu_0 H_0 = 0.1$ T. The two curves in the plot refer to two extreme propagation angles, for which the direction of propagation is parallel ($\theta = 0$) or perpendicular ($\theta = \pi/2$) to the direction of the saturation magnetization. The area between these two curves represents a manifold of SWs propagating at any angle.

As mentioned before, the propagation of SWs is determined by two types of interaction, the dipole and exchange interactions, which influence the magnetization dynamics in different wavenumber ranges. For small values of k the SW frequency does not depend on k, which is a characteristic feature of the magnetostatic waves in a homogeneous unbounded medium. For large values of k ($k \gtrsim 2 \times 10^7$ rad m^{-1}), where the dispersion relation is parabolic, the exchange interaction prevails over the dipole interaction. However, in the approach based on the LL equation (1) used in this paper, k has also an upper limit, as the LL equation

describes the SW dynamics with **m** being a continuous functions of the position and uses the approximate formula (4) for the exchange field. Thus, the applicability of this approach is limited to SWs with wavelengths much larger than the spacing between ferromagnetic atoms in the crystal lattice ($k \ll 1 \times 10^{10}$ rad m^{-1}).

This means that the relative strength of these two types of interaction will change with the wavelength of the spin waves ($\lambda = 2\pi/k$). The magnetization dynamics will be different in the two regimes, in which either the dipole or exchange interaction dominates; therefore, the SW spectrum will not follow the simple scaling rule that applies in photonics.[22]

An analytical theory of SWs in ferromagnetic thin films was developed by Kalinikos and Slavin in Ref. [29]. Following their approach, we will consider a magnetically saturated homogeneous ferromagnetic thin film of a thickness d, with the static magnetization vector **M** parallel to the static component $\mathbf{H}_{\text{eff},0}$ of the effective magnetic field (Fig. 1(b)).[114] A spin wave with an angular frequency ω and a wave vector **k** propagates in the plane of the film at an angle φ with respect to the direction of the vector $\mathbf{H}_{\text{eff},0}$ projected onto the film plane. The vectors $\mathbf{H}_{\text{eff},0}$ and **M** form an angle ϑ with the normal to the film plane. In the linear approximation the dispersion relation takes the form:[29]

$$\begin{aligned} \omega \;=\; & \gamma\mu_0 \left[(H_{\text{eff},0} + M_{\text{S}} l_{\text{ex}}^2 k^2) \right. \\ & \times \; \left. (H_{\text{eff},0} + M_{\text{S}} l_{\text{ex}}^2 k^2 + M_{\text{S}} F(\varphi,\vartheta)) \right]^{1/2}. \end{aligned} \tag{13}$$

The function $F(\varphi,\vartheta)$ is defined as:

$$F(\varphi,\vartheta) = P + \sin^2\vartheta \left[1 - P(1+\cos^2\varphi) + M_{\text{S}} \frac{P(1-P)\sin^2\varphi}{(H_0 + M_{\text{S}} l_{\text{ex}}^2)} \right], \tag{14}$$

where

$$P \;=\; 1 - \frac{1-\mathrm{e}^{-kd}}{kd}. \tag{15}$$

The contribution of the dipolar interaction to the spin-wave dynamics is expressed by $F(\varphi,\vartheta)$, defined in Eq. (14), and the effect of the exchange interaction is represented in Eq. (13) by the terms proportional to k^2. In the case considered here the static component of the effective magnetic field includes the external static magnetic field H_0 and the static demagnetizing field. For the two configurations discussed in this paper, i.e., for $\vartheta = 0$ and $\vartheta = 90°$, the static component of the effective magnetic field is $H_{\text{eff},0} = H_0 - M_{\text{S}}$, and $H_{\text{eff},0} = H_0$, respectively. The equation (13) was obtained for the unpinned magnetization

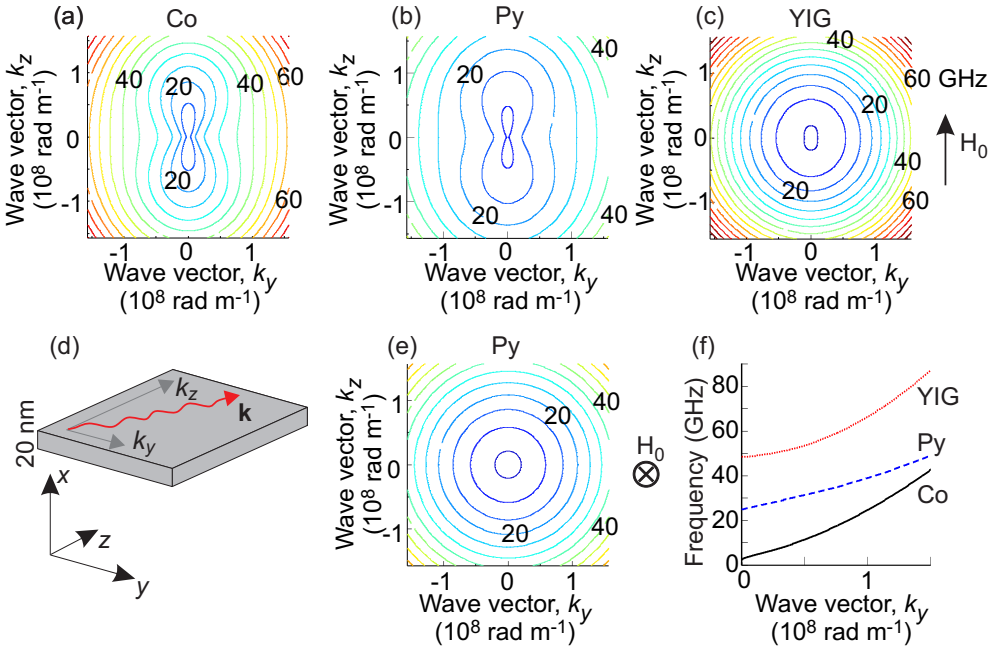

FIG. 3: Contours of constant frequency (iso-frequency plots) of SWs in a 20 nm thick ferromagnetic film. (a), (b), (c) Iso-frequency plots in Co, Py and yttrium iron garnet (YIG) films, respectively, with in-plane bias magnetic field $H_0 = 0.1$ T. (e) Iso-frequency plots in a Py thin film with a 1.1 T out-of-plane bias magnetic field. (f) Spin-wave dispersion along one selected in-plane direction in Co, Py and YIG films with an out-of-plane bias magnetic field.

dynamics on the surfaces of the film and under the assumption that the excitation amplitude is uniform across the film thickness. These two assumptions are fulfilled to a large extent in many recent experimental studies of thin-film MCs.[30–36] As compared to the parabolic and linear dispersion relations of electronic and electromagnetic waves, respectively, in homogeneous media, the SW dispersion relation $f(\mathbf{k})$ described by Eq. (13) has a complex and nonmonotonic dependence on the in-plane wave vector. The SW frequency depends on (i) the wavenumber k, (ii) the magnitude of the external magnetic field $\mathbf{H}_0$, and (iii) its orientation with respect to $\mathbf{k}$ and the film plane (angles φ and ϑ); apart from these, (iv) the magnetocrystalline anisotropy and (v) the magnetization configuration will add further important parameters in the $f(\mathbf{k})$ dependence.[25,26,29,37,38]

Three geometries tend to be studied: the Damon-Eshbach geometry (DE), the backward volume magnetostatic wave geometry (BVMW), and the forward volume magnetostatic wave geometry (FVMW).[26] In the DE and BVMW geometries the magnetic field $\mathbf{H}_0$ is oriented

in the plane of the film ($\vartheta = 90°$) and the propagation of SWs is perpendicular ($\varphi = 90°$) and parallel ($\varphi = 0$), respectively, to the direction of this field. In Fig. 3(a)-(c) these two propagation directions are the y and z directions, respectively. Since the dispersion relation depends on the angle φ, the dispersion is anisotropic. In the FVMW geometry the static component $\mathbf{H}_{\text{eff},0}$ of the effective magnetic field is perpendicular to the plane of the film ($\vartheta = 0$), the φ dependence drops out of the dispersion relation (13), and the propagation of SWs in the plane of the film is isotropic (see Fig. 3(e)).

Figure 3 shows the dispersion relation of SWs in a thin film with an in-plane magnetization over the k_y, k_z plane in the range $k_\text{y}, k_\text{z} \in (-1.57; 1.57) \times 10^8$ rad m^{-1} for 20 nm thick films of (a) cobalt (Co), (b) permalloy (Py), and (c) YIG (yttrium iron garnet, $Y_3Fe_5O_{12}$). The wave vector range in which the exchange interaction prevails over the dipolar interaction can be roughly determined from these diagrams, considering that exchange-dominated SWs have a parabolic and isotropic dispersion relation. In YIG the exchange interaction is dominant in most of the considered range (for $f > 10$ GHz, Fig. 3(c)), while in Co and Py the anisotropic dispersion indicates major contribution of the dipolar interaction even at $k \approx 10^8$ rad m^{-1} and $f \approx 40$ GHz, where the iso-frequency contours are elliptical. For small k_y the dispersion relation $f(k_\text{y})$ is monotonic and linear with a positive slope, which is characteristic of the DE geometry (Fig. 3(c)). However, the $f(k_\text{z})$ dependence is nonmonotonic; starting from $k_\text{z} = 0$ the frequency decreases with increasing wavenumber, attains a minimum and then increases with k_z. It is usually assumed that above the k value corresponding to the minimum the exchange interaction prevails over the magnetostatic interaction. Such a nonmonotonic dispersion relation is characteristic of the BVMW geometry.

In the FVMW geometry the static component $\mathbf{H}_{\text{eff},0}$ of the magnetic field is perpendicular to the film plane and the dispersion relation is isotropic regardless of the material. Nevertheless, exchange and dipole-exchange regimes can still be distinguished: the exchange-dominated part has a parabolic dispersion (Fig. 3(e)), whereas in the dipolar and dipole-exchange parts the k dependence of f is linear (Fig. 3(f)).

III. CALCULATIONS OF THE MAGNONIC BAND STRUCTURE

A. Bloch's theorem

Solutions of the LL equation in MC shall fulfill Bloch's theorem, which asserts that a solution of a differential equation with periodic coefficients can be represented as a product of a plane-wave envelope and a periodic function of the position vector. The properties of spin waves in MCs will have the same fundamental properties obtained from Bloch's theorem, which are common also with other excitations in periodic media, i.e., electrons in crystal lattice, electromagnetic waves in photonic crystals and elastic waves in phononic crystals.

According with this theorem dynamical components of the magnetization vector in LL equation (2) $[\mathbf{m}(\mathbf{r}) = m_x(\mathbf{r}) + m_y(\mathbf{r})]$ in MC, where all coefficients are periodic function of the position vector (with the lattice vector $\mathbf{a}$) can be written as a Bloch waves:

$$m_{x_i,\mathbf{k}}(\mathbf{r}) = \breve{m}_{x_i,\mathbf{k}}(\mathbf{r})\mathrm{e}^{i\mathbf{k}\cdot\mathbf{r}}, \tag{16}$$

where x_i stands for x or y, here. $\breve{m}_{x_i,\mathbf{k}}$ denotes the periodic part of the Bloch function for any $\mathbf{k}$:

$$\breve{m}_{x_i,\mathbf{k}}(\mathbf{r}) = \breve{m}_{x_i,\mathbf{k}}(\mathbf{r}+\mathbf{a}).$$

The quantity $\mathbf{k}$ introduced in Eq. (16) is a wave vector of the plane wave envelope (the Bloch wave vector), which has same dimensionality as the spatial periodicity. It is introduced also as an index, $\mathbf{m}_\mathbf{k}$, to enumerate solutions. However, $\mathbf{k}$ could not be directly related to the momentum, as opposed to a SW wave vector in homogeneous media, because the periodic part of the Bloch function $\breve{m}_{x_i,\mathbf{k}}(\mathbf{r})$, by itself, can have Fourier decomposition with any spectra of the wavelengths.[21] Thus, the $\mathbf{k}$ vector is called quasi-wave vector and it can be associated with the crystal momentum, rather than with SW momentum (only when there is no periodic change of any type in the structure, the crystal momentum is strictly equal to the SW momentum). The crystal momentum enters conservation law that governs elastic and inelastic scattering processes in the crystal. A photon (or neutron) with wave vector $\mathbf{q}$ which absorbs (excites) the SW changes the wavenumber according with the selection rule governed by the reciprocal lattice.

Bloch's theorem implies important properties, which are general and independent on the

particular solution. First,

$$\mathbf{m}_\mathbf{k}(\mathbf{r}+\mathbf{a}) = \breve{\mathbf{m}}_\mathbf{k}(\mathbf{r}+\mathbf{a})\mathrm{e}^{i\mathbf{k}\cdot\mathbf{r}}\mathrm{e}^{i\mathbf{k}\cdot\mathbf{a}} = \mathbf{m}_\mathbf{k}(\mathbf{r})\mathrm{e}^{i\mathbf{k}\cdot\mathbf{a}}, \tag{17}$$

i.e., the spatial distribution of the dynamical magnetization vector, when shifted by the lattice vector, is modulated only by the phase factor $\mathrm{e}^{i\mathbf{k}\cdot\mathbf{a}}$.[115]

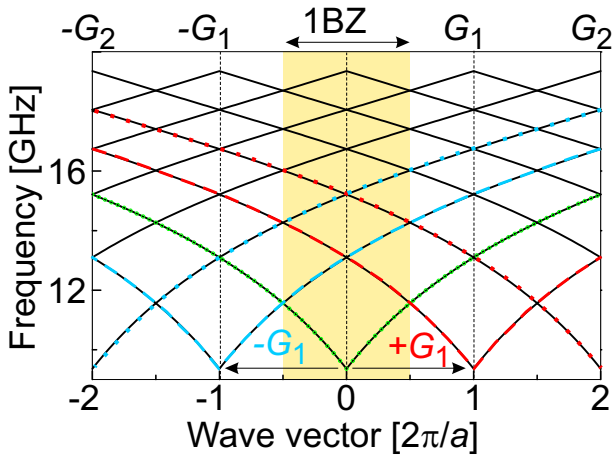

FIG. 4: Magnonic band structure in Py film of 20 nm thickness in the empty lattice model calculated with the plane wave method (PWM). The SW propagation is perpendicular to the in-plane magnetic field 0.1 T. The green circles show the dispersion of SW calculated from Eq. (13). The red (blue) dotted lines mark the dispersion translated by reciprocal lattice vector $G_2 = 4\pi/a$ to the left (right). The shaded area points at the first Brillouin zone (1BZ).

From the Bloch's theorem Eq. (16) it also arises, that if $\mathbf{m}_\mathbf{k}$ is a solution of the LL equation, then

$$\mathbf{m}_{\mathbf{k}+\mathbf{G}}(\mathbf{r}) = \breve{\mathbf{m}}_{\mathbf{k}+\mathbf{G}}(\mathbf{r})\mathrm{e}^{i(\mathbf{k}+\mathbf{G})\cdot\mathbf{r}} \tag{18}$$

is also a solution and identical with $\mathbf{m}_\mathbf{k}(\mathbf{r})$, where $\mathbf{G}$ is an arbitrary reciprocal lattice vector.[116] One of the most important consequences of Eq. (18) is, that solution $\mathbf{m}_\mathbf{k}(\mathbf{r})$ is associated with specific frequency $\omega(\mathbf{k})$. Since $\mathbf{m}_\mathbf{k}(\mathbf{r}) = \mathbf{m}_{\mathbf{k}+\mathbf{G}}(\mathbf{r})$, the dispersion relation in the wave vector space is also periodic:

$$\omega(\mathbf{k}) = \omega(\mathbf{k}+\mathbf{G}). \tag{19}$$

In Fig. 4 the dispersion curves of SWs in Py film for the DE configuration, which starts at $G_0 = 0$, $G_1 = \pi/a$, $-G_1$, $G_2 = 2\pi/a$ and $-G_2$ are shown. It means, that all possible values

of ω are already included in the range of $\mathbf{k} \in (-\pi/a; \pi/a)$. This is a back-folding (translation by the reciprocal lattice vector) of the dispersion relation into the first Brillouin zone (BZ). In the first BZ the dispersion relation is a multivalued function forming frequency bands, which formally comes from larger $\mathbf{k}$. Every frequency band and associated solution shall be indexed with integer n. However, for the simplicity we omit the band number $\mathbf{m}_{\mathbf{k}} \equiv \mathbf{m}_{\mathbf{k},n}$. It is sufficient in the theoretical investigations to consider the first BZ only.

The MC with desired spectrum can be obtained by appropriate adjustment of the structure and materials in the fabrication process and also in the later stage by the change of the magnetization configuration or modulation introduced by the external magnetic field. Similarly to the dispersion in homogeneous ferromagnetic thin films, the dispersion relation in MCs will depend on the film thickness, the magnitude of the magnetic field, and its direction. However, for a given material and film thickness, the lattice constant a of the MC determines whether the boundary of the first BZ (e.g., $k = \pi/a$ in a 1D MC or a 2D MC based on a square lattice with a lattice constant a) will be in the magnetostatic or exchange-dominated regime. Thus, for relatively large and medium lattice constants the BZ boundary (and back-folding) will take place in the magnetostatic regime of $\omega(k)$. For small values of a the boundary of the first BZ is in the exchange regime. The dispersion relation in thin films is anisotropic and in 2D MC the folding effect will make band structure more complicated. The formation of the band structure in these crystals will be described in Sec. IV A 2.

B. Plane wave method

The plane wave method (PWM) is well suited to solve the wave equation in a periodic media, which fully exploits the Bloch theorem. It has been successfully implemented in calculations of photonic and phononic band structures in photonic and phononic crystals,[22] respectively, as well as electronic band structures in crystals and semiconductor heterostructures.[21,39–41] We applied this method to calculate magnonic band structure in MCs. However, before presentation of the PWM for SW's calculations, we will derive formulas for two main components of the effective magnetic field from Eq. (3) in piecewise constant, periodic magnetic structures, i.e., in MCs. These are the exchange and magnetostatic fields, required in PWM calculations.

1. Exchange field in magnonic crystals

The exchange field defined in Eq. (4) in linear approximation for homogeneous ferromagnetic film needs modification. We limit consideration of the exchange field to MCs with collinear and piecewise constant static magnetization distribution.

The microscopic source of the exchange interaction is the quantum mechanical Pauli exclusion principle for electrostatically interacting electrons with spins. This interaction between two localized spins $\mathbf{S}_l$ and $\mathbf{S}_m$ is effectively described by the dot product of these spins, $\mathbf{S}_l \cdot \mathbf{S}_m$. Thus, the interaction of the selected spin on site l with the lattice of spins is described by the Heisenberg Hamiltonian:

$$H_l = -\sum_{m \in \mathrm{NN}} J_{l,m} \mathbf{S}_l \cdot \mathbf{S}_m, \tag{20}$$

where the strength of the exchange interaction is given by the exchange integral $J_{l,m}$. The summation in Eq. (20) is limited to the nearest neighbors (NN) spins of the l-th spin only. The unit directional vector of the spin, α_l, can be used to relate spins on discrete lattice to the magnetization being a continuous function of the position vector:

$$\alpha_l = \frac{\mathbf{S}_l}{|\mathbf{S}_l|} = \frac{\mathbf{M}(\mathbf{r}_l)}{|\mathbf{M}(\mathbf{r}_l)|}, \tag{21}$$

where $\mathbf{M}(\mathbf{r}) = N_\mathrm{S} \mu_\mathrm{B} g \mathbf{S}_l$ (N_S is the number of spins in the unit cell volume, μ_B is Bohr magneton and g is g-factor). In the limit of small deviations of the neighboring spins, the α_m can be expanded into Taylor series around orientation of α_l. Limiting this expansion to the quadratic terms and substitution to Eq. (20) gives us the expression for the exchange energy density:[42,43]

$$\epsilon_\mathrm{ex} = \lambda_\mathrm{w} M^2 + A \sum_{i=1}^{3} \left(\frac{\partial \alpha}{\partial x_i} \right)^2, \tag{22}$$

where x_i enumerates Cartesian components x, y and z. We assumed here, that exchange integrals between any neighboring spins are the same, $J_{i,j} \equiv J$, and in case of considered here ferromagnetic materials it has positive sign. The expression $\lambda_\mathrm{w} M^2$ has meaning of the Weiss field. The material parameters λ_w and A are linked to the microscopic parameters by the relations:

$$\lambda_\mathrm{w} = \frac{-2ZJ}{N_\mathrm{S} \mu_\mathrm{B}^2 g^2}, \quad A = \frac{2 J n_\mathrm{l} S^2}{a}, \tag{23}$$

where $n_\mathrm{l} = 1$, 2, or 4 for sc, bcc, or fcc lattice, respectively and Z is a number of NNs (6, 8 and 12, for sc, bcc and fcc, respectively). The integration of the energy density ϵ_ex over the volume of the magnetic material gives the exchange energy:

$$E_\mathrm{ex} = \int_V \epsilon_\mathrm{ex} dV. \tag{24}$$

To find the exchange field entering LL equation (2) we have to calculate the functional derivative of E_ex with respect to the magnetization vector:[37]

$$\mathbf{H}_\mathrm{ex} = -\frac{1}{\mu_0}\frac{\delta E_\mathrm{ex}}{\delta \mathbf{M}}. \tag{25}$$

The following formula is derived:

$$\mathbf{H}_\mathrm{ex} = \nabla l_\mathrm{ex}^2 \nabla \mathbf{m}, \tag{26}$$

where l_ex is exchange length defined in Eq. (5). This formula is derived in linear approximation, adequate for calculation of the magnonic band structure. It reduces to the Eq. (4) in case of a homogeneous material. Although the exchange field was derived from the Heisenberg model, which assumes localized spins on the discrete lattice, it describes also very well the magnetization dynamics in ferromagnetic metals and dielectrics. The important issue is contribution of interfaces between different materials. The boundary condition problem was discussed in Ref. [44], where ambiguity in the derivation of the formula for exchange field was discussed. However, for bi-component magnonic crystals composed of Py and Co the difference between proposed formulations of the exchange field is minor, due to the similar values of the exchange length. Nevertheless, the general formulation of the exchange field in inhomogeneous magnetic materials still needs to be developed, especially having in mind the various possible contributions affecting spin wave dynamics at the interfaces.[45]

2. Formulation of the eigenproblem

With exchange field defined in inhomogeneous ferromagnetic material [Eq. (26)] we can write explicitly LL equation (1). If we assume that the magnetization saturation, although space dependent, is everywhere along z axis, the linearized LL equation takes the following

form:

$$
\begin{aligned}
& i\frac{\omega}{\gamma\mu_0}m_x(\mathbf{r}) = -M_{\rm S}(\mathbf{r})[\nabla\cdot l_{\rm ex}(\mathbf{r})\nabla]m_y(\mathbf{r}) \\
+\ & m_y(\mathbf{r})\left[H_0 + H^{\rm ms}(\mathbf{r})\right] - M_{\rm S}(\mathbf{r})h_y^{\rm ms}(\mathbf{r}), \qquad (27)\\
& i\frac{\omega}{\gamma\mu_0}m_y(\mathbf{r}) = M_{\rm S}(\mathbf{r})[\nabla\cdot l_{\rm ex}(\mathbf{r})\nabla]m_x(\mathbf{r}) \\
-\ & m_x(\mathbf{r})\left[H_0 + H^{\rm ms}(\mathbf{r})\right] + M_{\rm S}(\mathbf{r})h_x^{\rm ms}(\mathbf{r}). \qquad (28)
\end{aligned}
$$

We have assumed here that, the space dependent magnetostatic field is composed with static $H^{\rm ms}(\mathbf{r})$ and dynamic parts $\mathbf{h}^{\rm ms}(\mathbf{r})$:

$$\mathbf{H}^{\rm ms}(\mathbf{r}) = H^{\rm ms}(\mathbf{r})\hat{z} + h_x^{\rm ms}(\mathbf{r})\hat{x} + h_y^{\rm ms}(\mathbf{r})\hat{y}. \qquad (29)$$

The magnetostatic field components for the planar MC are derived in Sec. III B 3.

To solve Eqs. (27)-(28) we expand all periodic coefficients (in our case $M_{\rm S}$ and $l_{\rm ex}$) in Fourier series to map them onto the reciprocal space:

$$
\begin{aligned}
M_{\rm S}(\mathbf{r}) &= \sum_j M_{\rm S}(\mathbf{G}_j)e^{i\mathbf{G}_j\cdot\mathbf{r}}, \\
l_{\rm ex}(\mathbf{r}) &= \sum_j l_{\rm ex}(\mathbf{G}_j)e^{i\mathbf{G}_j\cdot\mathbf{r}}, \qquad (30)
\end{aligned}
$$

where summation is over reciprocal lattice vectors $\mathbf{G}_j$. $M_{\rm S}(\mathbf{G}_j)$ and $l_{\rm ex}(\mathbf{G}_j)$ are Fourier coefficients indexed with the reciprocal lattice vector $\mathbf{G}_j$. They can be calculated analytically or numerically from the inverse Fourier transform:

$$M_{\rm S}(\mathbf{G}_j) = \frac{1}{V_{\rm C}}\int_{V_{\rm C}} M_{\rm S}(\mathbf{r})\mathrm{e}^{-i\mathbf{G}_j\cdot\mathbf{r}}dv, \qquad (31)$$

where the integration is over the the unit cell $V_{\rm C}$ (i.e., over volume, area and segment in 3D, 2D and 1D MCs, respectively).

In 1D MCs [Fig. 5] $\mathbf{G} = (G, 0) = (\frac{2\pi}{a}n, 0)$ where n is integer and a is lattice constant. The formula for the Fourier coefficients $M_{\rm S}(\mathbf{G}_j)$ is following:

$$M_{\rm S}(\mathbf{G}_j) = \begin{cases} \Delta M_{\rm S}\frac{a_A}{a} + M_{\rm S,B}, & \text{for } G_j = 0, \\ \Delta M_{\rm S}\frac{a_A}{a}\frac{\sin\frac{G_j a_A}{2}}{\frac{G_j a_A}{2}}, & \text{for } G_j \neq 0, \end{cases} \qquad (32)$$

where $\Delta M_{\rm S} = M_{\rm S,A} - M_{\rm S,B}$, a_A is the width of the stripe of material A, $M_{\rm S,A}$ and $M_{\rm S,B}$ are magnetization saturation of material A and B, respectively. The similar formula are for $l_{\rm ex}(\mathbf{G}_j)$.

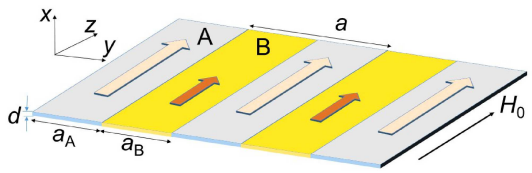

FIG. 5: 1D planar MC composed of regular array of stripes made from two ferromagnetic materials A and B. Materials are saturated along the stripe axis by external magnetic field H_0, the stripes widths are a_A and a_B, respectively, the period is a.

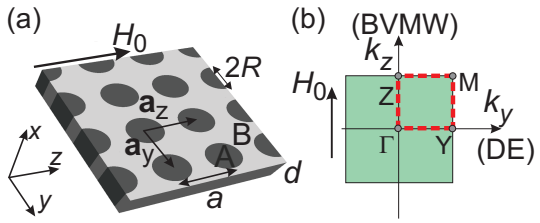

FIG. 6: (a) Bi-component MC of square lattice formed by A circular dots of radius R included in host material B. The thickness of the MC is d, the lattice constant is a. The magnetic field H_0 is oriented along the z-axis. (b) First Brillouin zone (BZ) for the structure shown in (a), with indicated high-symmetry points Γ, Y, M and Z in the center and at the border of the first BZ. We distinguish the two directions of the wave vector $\mathbf{k}$ along the bias magnetic field and perpendicular to it, i.e., the backward volume magnetostatic wave (BVMW) and Damon-Eshbach (DE) geometry, respectively.

In a square lattice the reciprocal lattice vectors are: $\mathbf{G} = (G_y, G_z) = \frac{2\pi}{a}(n_y, n_z)$, where n_y, and n_z are integers. In the case of cylindrical dots [Fig. 6] the Fourier components of the saturation magnetization $M_{\rm S}(\mathbf{G}_i)$ are calculated analytically from Eq. (31):

$$M_{\rm S}(\mathbf{G}_j) = \begin{cases} \Delta M_{\rm S} \frac{\pi R^2}{a^2} + M_{\rm S,B}, & \text{for } \mathbf{G}_j = 0, \\ 2\Delta M_{\rm S} \frac{\pi R^2}{a^2} \frac{J_1(G_j R)}{G_j R}, & \text{for } \mathbf{G}_j \neq 0, \end{cases} \tag{33}$$

where J_1 is a Bessel function of the first kind, R is a radius of the dot. G_j is the length of the reciprocal lattice vector $\mathbf{G}_j$.

The Fourier transformation is also applied to $H^{\rm ms}(\mathbf{r})$, which has the same period as MC, and to periodic parts of the dynamical components of the magnetization vector and magnetostatic field defined in Eqs. (16) and (29). Then the Fourier representations of $\mathbf{m}_{\mathbf{k}}(\mathbf{r})$

and $\mathbf{h_k}(\mathbf{r})^{\rm ms}$ are:

$$\begin{aligned}\mathbf{m_k}(\mathbf{r}) &= \sum_j \mathbf{m_k}(\mathbf{G}_j)\mathrm{e}^{i(\mathbf{k}+\mathbf{G}_j)\cdot\mathbf{r}} \\ \mathbf{h}_\mathbf{k}^{\rm ms}(\mathbf{r}) &= \sum_j \mathbf{h}_\mathbf{k}^{\rm ms}(\mathbf{G}_j)\mathrm{e}^{i(\mathbf{k}+\mathbf{G}_j)\cdot\mathbf{r}}. \end{aligned} \tag{34}$$

$\mathbf{m_k}(\mathbf{G}_j)$ and $\mathbf{h}_\mathbf{k}^{\rm ms}(\mathbf{G}_j)$ are Fourier coefficients indexed with the reciprocal lattice vector $\mathbf{G}_j$.

By substituting Eqs. (30) and (34) into the equations (27)-(28) we transform LL equation into the algebraic eigenproblem:

$$\hat{M}(\mathbf{k})\mathbf{m_k}(\mathbf{G}) = i\Omega\mathbf{m_k}(\mathbf{G}), \tag{35}$$

where reduced frequency $\Omega = \omega/(\gamma\mu_0 H_0)$ is the eigenvalue and $\mathbf{m_k}(\mathbf{G})$ stands for the eigenvector of elements:

$$\begin{aligned}\mathbf{m_k}(\mathbf{G}) &= [\mathbf{m}_{x,\mathbf{k}}(\mathbf{G}), \mathbf{m}_{y,\mathbf{k}}(\mathbf{G})] \\ &= [m_{x,\mathbf{k}}(\mathbf{G}_1), m_{x,\mathbf{k}}(\mathbf{G}_3), \cdots, m_{x,\mathbf{k}}(\mathbf{G}_N), \\ &\quad m_{y,\mathbf{k}}(\mathbf{G}_1), m_{y,\mathbf{k}}(\mathbf{G}_3), \cdots, m_{y,\mathbf{k}}(\mathbf{G}_N)]\,. \end{aligned} \tag{36}$$

There, N reciprocal lattice vectors, usually of the shorter length, have been used in the expansions (30) and (34) to get finite set of algebraic equations suitable for numerical solution.

The matrix $\hat{M}$ is the block matrix:

$$\hat{M} = \begin{pmatrix} M^{xx} & M^{xy} \\ M^{yx} & M^{yy} \end{pmatrix}, \tag{37}$$

with submatrices defined as follows:

$$M_{ij}^{xx} = M_{ij}^{yy} = 0,$$

$$\begin{aligned} M_{ij}^{xy} &= \delta_{ij} - \frac{h_y^{\rm ms}(\mathbf{G}_{i-j})}{H_0} + \frac{H^{\rm ms}(\mathbf{G}_{i-j})}{H_0} \\ &+ \sum_l \frac{(\mathbf{k}+\mathbf{G}_j)\cdot(\mathbf{k}+\mathbf{G}_l)}{H_0} l_{\rm ex}^2(\mathbf{G}_{l-j}) M_{\rm S}(\mathbf{G}_{i-l}), \end{aligned}$$

$$\begin{aligned} M_{ij}^{\rm xy} &= -\delta_{ij} + \frac{h_x^{\rm ms}(\mathbf{G}_{i-j})}{H_0} - \frac{H^{\rm ms}(\mathbf{G}_{i-j})}{H_0} \\ &- \sum_l \frac{(\mathbf{k}+\mathbf{G}_j)\cdot(\mathbf{k}+\mathbf{G}_l)}{H_0} l_{\rm ex}^2(\mathbf{G}_{l-j}) M_{\rm S}(\mathbf{G}_{i-l}), \end{aligned}$$

where $\mathbf{G}_{i-j} \equiv \mathbf{G}_i - \mathbf{G}_j$. We have assumed that the magnetostatic field defined here has contribution only along axis related to its component.

To compute the dispersion relation of SWs $\omega(\mathbf{k})$ we have to solve eigenproblem (35) for successive values of $\mathbf{k}$ along the irreducible part of the first BZ, for the square lattice this is along the path marked in Fig. 6(b) with dashed line. Numerically, Eq. (35) can be solved only for the finite number of terms (N) in the Fourier expansions [Eqs. (30) and (34)]. This number needs to be chosen sufficiently large to guarantee converged results.

3. Demagnetizing field

The remaining factor which needs to be evaluated before solving numerically eigenproblem (35) is a magnetostatic field, formally introduced in Eq. (29). In general, both static and dynamic parts of this field are inhomogeneous. In MC, even at saturation, the magnetization is inhomogeneous, thus $\nabla \cdot \mathbf{M} \neq 0$.

Magnetostatic field can be defined as a gradient of the magnetostatic potential: $\mathbf{H}^{\mathrm{ms}} = -\nabla\psi$, where $\mathbf{H}^{\mathrm{ms}}$ has static and dynamic components according with Eq. (29).[117] The magnetostatic field can be derived from the solution of the Poisson equation for the magnetostatic potential ψ:

$$\nabla^2\psi + \rho_{\mathrm{M}} = 0, \tag{38}$$

where $\rho_{\mathrm{M}} = -\nabla \cdot \mathbf{M}$ can be interpreted by analogy with electrostatic, as an effective density of the magnetic charges. The solution of Eq. (38) can be written as:[46]

$$\psi(\mathbf{r}) = -\frac{1}{4\pi}\int \frac{\nabla' \cdot \mathbf{M}(\mathbf{r}')}{|\mathbf{r}-\mathbf{r}'|} d^3r', \tag{39}$$

where integration is over whole space and ∇' means differential operator with respect to $\mathbf{r}'$.

We can split the integration in Eq. (39) into two terms according with the Gauss theorem:

$$\psi(\mathbf{r}) = -\frac{1}{4\pi}\left[\int_V \frac{\nabla' \cdot \mathbf{M}(\mathbf{r}')}{|\mathbf{r}-\mathbf{r}'|} d^3r' - \oint_S \frac{\mathbf{M}(\mathbf{r}') \cdot \mathbf{n}}{|\mathbf{r}-\mathbf{r}'|} dS'\right]. \tag{40}$$

The first integral is over entire volume of the magnetic body V, the second term is integral over the surface of the magnetic body S, $\mathbf{n}$ is the unit vector which points at direction normal to the surface. In case of homogenous magnetization $\nabla \cdot \mathbf{M} = 0$ and only the second term contribute to $\mathbf{H}^{\mathrm{ms}}$. In this case a demagnetizing field inside of the body and stray

magnetic field outside of the body can be interpreted as a result of the surface magnetic charges.

Here, we use different approach, which is based on solution of Eq. (39) in plane wave basis.[47] With integration by parts, the solution (39) can be transformed to the form:[46]

$$\begin{aligned}\psi(\mathbf{r}) &= \frac{1}{4\pi}\left[-\int \nabla'\cdot\left(\frac{\mathbf{M}(\mathbf{r}')}{|\mathbf{r}-\mathbf{r}'|}\right)d^3r'\right.\\ &+ \left.\int \mathbf{M}(\mathbf{r}')\cdot\nabla'\frac{1}{|\mathbf{r}-\mathbf{r}'|}d^3r'\right].\end{aligned} \tag{41}$$

The integration is extended over whole space here. According with the divergence theorem, the first term is transformed into integral over the closed surface. Because this surface is outside of the magnetic material, it can be in infinity, this term vanishes. Taking into account that $\nabla'\left(1/|\mathbf{r}-\mathbf{r}'|\right) = -\nabla\left(1/|\mathbf{r}-\mathbf{r}'|\right)$, the second term can be rewritten:

$$\begin{aligned}\psi(\mathbf{r}) &= -\frac{1}{4\pi}\nabla\cdot\int\frac{\mathbf{M}(\mathbf{r}')}{|\mathbf{r}-\mathbf{r}'|}d^3r'\\ &= -\sum_{x_i=x,y,z}\nabla_{x_i}\left[\frac{1}{4\pi}\int\frac{M_{x_i}(\mathbf{r}')}{|\mathbf{r}-\mathbf{r}'|}d^3r'\right].\end{aligned} \tag{42}$$

One can notice that the integral inside of the Eq. (42):

$$\Phi_{x_i}(\mathbf{r}) \equiv \frac{1}{4\pi}\int\frac{M_{x_i}(\mathbf{r}')}{|\mathbf{r}-\mathbf{r}'|}d^3r' \tag{43}$$

is formally a solution of the Poisson equation inside of the MC:

$$\nabla^2\Phi^{\text{in}}_{x_i}(\mathbf{r}) = -M_{x_i}, \tag{44}$$

which outside of the MC takes the form of the Laplace equation:

$$\nabla^2\Phi^{\text{out}}_{x_i}(\mathbf{r}) = 0. \tag{45}$$

Because $\Phi_{x_i}(\mathbf{r})$ fulfills Eqs. (44) and (45), thus by analogy with electrostatic potential,[46] the magnetization component from the right hand side of Eq. (44) can be interpreted as a density of magnetic charges and Φ_{x_i} as a potential due to these charges.

Eqs. (44) and (45) accompanied with boundary conditions at the MC film surfaces $x = \pm d/2$:

$$\Phi^{\text{in}}_{x_i} = \Phi^{\text{out}}_{x_i} \text{ and } \frac{\partial\Phi^{\text{in}}_{x_i}}{\partial x} = \frac{\partial\Phi^{\text{out}}_{x_i}}{\partial x}$$

are used to derive the formula for density of the magnetic charges inside of the magnetic film $\Phi^{\text{in}}_{x_i}$. Here, we follow the expansions into the Fourier series of the static component of

the magnetization vector $M_z \equiv M_\mathrm{S}$ and exploiting the Bloch theorem with Fourier series for dynamical components of the magnetization, i.e., m_x and m_y. The respective magnetic densities follow similar transformations, i.e., $\Phi_z^{\mathrm{in(out)}}$ Fourier expansion, $\Phi_x^{\mathrm{in(out)}}$ and $\Phi_y^{\mathrm{in(out)}}$ using Bloch theorem with the Fourier expansion of the periodic parts. For Φ inside of the MC we get:

$$\begin{aligned}
\Phi_z^{\mathrm{in}}(\mathbf{r}) &= \sum_j M_\mathrm{S}(\mathbf{G}_j)\frac{1-\cosh(G_j x)\mathrm{e}^{G_j d}}{G_j^2}\mathrm{e}^{i\mathbf{G}_j\cdot\mathbf{r}} \\
\Phi_{x,(y)}^{\mathrm{in}}(\mathbf{r}) &= \sum_j m_{\mathbf{k},x(y)}(\mathbf{G}_j)\frac{1-\cosh(|\mathbf{k}+\mathbf{G}_j|x)\mathrm{e}^{|\mathbf{k}+\mathbf{G}_j|d}}{(\mathbf{k}+\mathbf{G}_j)^2} \\
&\quad\times\mathrm{e}^{i(\mathbf{k}+\mathbf{G}_j)\cdot\mathbf{r}}.
\end{aligned} \tag{46}$$

According with Eq. (42) the divergence of Φ provides the magnetostatic potential ψ, from which the magnetostatic field components can be directly calculated.[48,49]

For the considered structure, each component of the magnetization vector can contribute to each component of the magnetostatic field $\mathbf{H}^{\mathrm{ms}}$, however we will limit here only to the fields related to the same components of the magnetization. With this approximation we get the following expression for the static and dynamical components of the magnetostatic field in planar MC:

$$\begin{aligned}
H^{\mathrm{ms}}(\mathbf{r},x) &= \sum_j H^{\mathrm{ms}}(\mathbf{G}_j,x)\mathrm{e}^{i\mathbf{G}_j\cdot\mathbf{r}} \qquad (47)\\
&= -\sum_j M_\mathrm{S}(\mathbf{G}_j)\frac{{G_{z,j}}^2}{\mathbf{G}_j^2}A(\mathbf{G}_j,x)\mathrm{e}^{i\mathbf{G}_j\cdot\mathbf{r}}, \\
h_x^{\mathrm{ms}}(\mathbf{r},x) &= \sum_j h_x^{\mathrm{ms}}(\mathbf{G}_j,x)\mathrm{e}^{i(\mathbf{k}+\mathbf{G}_j)\cdot\mathbf{r}} \qquad (48)\\
&= -\sum_j m_\mathrm{x}(\mathbf{G}_j)C(\mathbf{k}+\mathbf{G}_{x,j},x)\mathrm{e}^{i(\mathbf{k}+\mathbf{G}_j)\cdot\mathbf{r}}, \\
h_y^{\mathrm{ms}}(\mathbf{r},x) &= \sum_j h_y^{\mathrm{ms}}(\mathbf{G}_{x,j})\mathrm{e}^{i(\mathbf{k}+\mathbf{G}_j)\cdot\mathbf{r}} \qquad (49)\\
&= -\sum_j m_\mathrm{y}(\mathbf{G}_j)\frac{(k_y+G_{y,j})^2}{|\mathbf{k}+\mathbf{G}_j|^2}A(\mathbf{k}+\mathbf{G}_{x,j},x) \\
&\quad\times\mathrm{e}^{i(\mathbf{k}+\mathbf{G}_j)\cdot\mathbf{r}},
\end{aligned}$$

where the functions: $C(\kappa,x)$, $A(\kappa,x)$ are defined as: $C(|\kappa|,x) = \cosh(|\kappa|x)\mathrm{e}^{-|\kappa|d/2}$ and $A(\kappa,x) = 1-\sinh(|\kappa|x)\mathrm{e}^{-|\kappa|d/2}$.

The obtained formulas for the demagnetizing fields are represented in the reciprocal space for the in-plane components, but depend also on the position across the thickness of the slab. However, when the slab is thin enough (which is the case for structures studied in this paper), the non-uniformity of the demagnetizing fields across the thickness can be neglected, and respective values of fields from Eqs (49) with $x = d/2$ are taken in our calculations.[50] Because of its Fourier series form, the solution found for the demagnetizing fields can be used directly in the Eq. (35).

C. Micromagnetic simulations

Before presenting magnonic band structures in thin-film MCs, we introduce also other method of the magnonic band structure calculation, it is micromagnetic simulations (MS) being kind of numerical experiments.[51–54] For the other methods of SW dispersion relation calculations, like a dynamical matrix method or method based on finite element method in the frequency domain we refer to the literature.[55,56]

Micromagnetic simulations are effective and widely used in studies of the magnetization dynamics in nanopatterned magnetic systems. The method is based on solving numerically full Landau-Lifshitz equation in time domain and real space using finite difference method (FDM) or finite elements method (FEM). Studies of magnetization dynamics are complex and time consuming tasks, therefore, correct planing of simulation process is important. In optimal case one simulation should give us full information about SWs dynamics in the studied structure, also allows to reproduce full, accurate dispersion relation and spin wave amplitude distribution.

In this paragraph we present the technique used to obtain dispersion relations with micromagnetic simulations. At the beginning typical technical details considering proper spin waves excitation and sampling of obtained results are discussed. Then, the algorithm of dispersion relation calculations and the algorithm of visualization of the particular modes is described. At the end of this section, a short introduction to much faster, and easier technique of obtaining ferromagnetic resonance (FMR) spectra and visualization of the modes corresponding to resonance frequencies is presented.

In studies of spin waves dynamics micromagnetic simulations are performed in two stages.

First, so-called static stage, during which stable, static magnetic configuration is achieved. This is because, the calculations of the spin wave dynamics should be initiated from equilibrium magnetic configuration to fulfill conditions of the linear approximation. Aim of second stage, called dynamic stage, is study of the spin wave dynamics under influence of the disturbing factor, e.g., dynamic magnetic field. Results of the second stage can be further used to reproduce dispersion relation of spin waves and also spatial distribution of the spin wave amplitude. We will concentrate on the second stage, directly connected with calculation of the SW dynamics, we will describe SW excitations suitable to calculation of the dispersion relation, and describe the post processing of data acquired during simulations.

1. Excitation of spin waves

The simplest method of the SWs excitation is by introducing a small, dynamic magnetic field (we denote its amplitude as $\mathbf{h}_0$), which is perpendicular to the effective magnetic field. This field should vary in time and space, while its spectrum in frequency space defines efficiency of excitation of spin waves at particular frequencies and wave vectors.[57] Proper definition of that field is crucial to excite all required modes with sufficient efficiency needed to reproduce full dispersion relation with high quality. In an ideal case all SWs should be excited with the same, or at least comparable efficiency, for interesting range of frequencies and wave vectors. For this purpose very useful is function which takes form of the window function in Fourier space, more precisely sinc function: $\mathrm{sinc}(\kappa_{\mathrm{cut}}\xi) = \sin(\kappa_{\mathrm{cut}}\xi)/(\kappa_{\mathrm{cut}}\xi)$, which has flat Fourier spectra in the κ space in the range $(-\kappa_{\mathrm{cut}}, \kappa_{\mathrm{cut}})$: $\mathcal{F}_\xi\left\{\mathrm{sinc}(\kappa_{\mathrm{cut}}\xi)\right\} = \Theta_{\mathrm{H}}\left(\kappa_+\kappa_{\mathrm{cut}}\right)\Theta_{\mathrm{H}}\left(-\kappa_+\kappa_{\mathrm{cut}}\right)$, where Θ_{H} is Heaviside step function. Therefore, to excite SWs we will use dynamic magnetic fields in the form:

$$\mathbf{h}_{\mathrm{dyn}}(\mathbf{r}, t) = \mathbf{h}_0 \mathrm{sinc}\left(k_{\mathrm{cut}}\rho\right)\mathrm{sinc}\left(2\pi f_{\mathrm{cut}}t\right)g(\mathbf{r}), \tag{50}$$

where ρ is a distance from point of the excitation, its form depends on required dimensionality of the excited waves and MCs, i.e. in case of 1D MCs and waves propagating in the direction of periodicity x: $\rho = x$, in case of 2D MCs and waves propagating in the plane of the periodicity (x, y): $\rho = \sqrt{x^2 + y^2}$; and in 3D MCs and omnidirectional waves $\rho = \sqrt{x^2 + y^2 + z^2}$. Values of parameters k_{cut} and f_{cut} are cut-off wave number and cut-off frequency, respectively. $g(\mathbf{r})$ is additional space dependent function. When antisymmetric

modes aren't taken into consideration, the constant $g(\mathbf{r})$ can be used, $g(\mathbf{r}) = 1$.[58,59] However, whenever the antisymmetric modes are required, there should be applied space dependent form of that coefficient. For example, the function $g(\mathbf{r}) = \eta(x)\eta(y)\eta(z)$ can be used,[60] with:

$$\eta(x_i) = \sum_{\zeta=1}^{N_\mathrm{A}} \left[\sin(2\pi x_i \zeta/a) - \cos(2\pi x_i \zeta/a)\right], \tag{51}$$

where x_i stands for x, y or z. For calculations of the low frequency magnonic bands the value N_A can be low (order 5 is enough to obtain good excitation of the antisymmetric modes).

2. Sampling

After excitation, very important technical issue to obtain proper dispersion relation is a sampling. Its parameters will determine accuracy of obtained dispersion relation and size of computational problem necessary to solve during post-processing of the simulation results.

Results of micromagnetic simulations can be represented in the form of 4 dimensional matrix $\hat{\mathbf{M}}(t, x, y, z)$ containing whole information about magnetization dynamics during simulations process sampled with time interval t_sampl and space interval $x_{i,\mathrm{sampl}}$. Size of the matrix (its dimension) is determined by sampling intervals (in space and time) and also by total size of the simulated system, as well as total time of the simulation. From computational reasons, it is important to use the matrix $\hat{\mathbf{M}}(t, x, y, z)$ with dimensions as small as possible, however simultaneously allowing to obtain clear and accurate dispersion relation. Too short choose of sampling intervals can result in achieving enormous size of matrices $\hat{\mathbf{M}}(t, x, y, z)$ which can be to big for farther processing due to limited computer resources. Moreover, improving data storing precision has sense only until some limit. After some limit, making too small time and space intervals (storing more points in space and time), doesn't improve visibly accuracy of the obtained dispersion.

Sampling intervals determine maximal values of the wave vector components k_i and frequency f available in the Fourier space, i.e. $k_{i,\max} = \pi/x_{i,\mathrm{sampl}}$ and $f_\mathrm{max} = 1/(2t_\mathrm{sampl})$. Size of the matrix $\hat{\mathbf{M}}(t, x, y, z)$ defines resolution of the image obtained in wave vector and frequency domain [$\Delta k_{i,x} = k_{i,\max}/(2\dim_i \hat{\mathbf{M}}(t, x, y, z))$, $\Delta f = f_\mathrm{max}/(2\dim_t \hat{\mathbf{M}}(t, x, y, z))$, where operator $\dim_i$ and $\dim_t$ gives dimension of the matrix along i-th dimension $i \in \{x, y, z\}$, and time, respectively].

Next issue is a number of points in dispersion relation along k_i axis inside the first Brillouin zone. This number is equal to half of the total periods along the i-th axis used in simulations. Therefore, to obtain precise dispersion relation it is necessary to simulate sufficiently long structure, in practice consisted at least several dozen periods. To summarize, non-homogeneity of the exciting dynamic magnetic field and the structure long for many periods is essential to get dispersion relation. Periodic boundary conditions (as defined in micromagnetic simulations, i.e., by making finite number of copies of the unit cells) cannot be used to limit size of simulated area in directions of periodicity. However, applying periodic boundary conditions (PBC) can be used to other purposes, i. e. to avoid influence of the demagnetizing field from edges of the considered structure.

3. Dispersion relation calculation

From the matrix $\hat{\mathbf{M}}(t, x, y, z)$, obtained from micromagnetic simulations, we can calculate dispersion relation of SWs. General algorithm of calculating magnonic band structure is presented in Fig. 7(a). In the first step we choose one component of the magnetization vector, i.e., the i-th component of the matrix, $\hat{M}_i(t, x, y, z)$. Then, we calculate Fast Fourier Transform (FFT), $\mathcal{F}_d$ (where d denotes dimension over which FFT is computed) of that matrix over required dimensions, i.e. in the case of 1D MC over time t and direction of the periodicity x:

$$\widetilde{M}_i(f, k_x, y, z) = \mathcal{F}_{t,x}\left\{\hat{M}_i(t, x, y, z)\right\} \tag{52}$$

and

$$\widetilde{M}_i(f, k_x, k_y, z) = \mathcal{F}_{t,x,y}\left\{\hat{M}_i(t, x, y, z)\right\}, \tag{53}$$

$$\widetilde{M}_i(f, k_x, k_y, k_z) = \mathcal{F}_{t,x,y,z}\left\{\hat{M}_i(t, x, y, z)\right\} \tag{54}$$

in 2D and 3D MCs, respectively.

In the structures with periodicity along one direction and finite extend in the perpendicular plane, e.g., in the SW waveguides with periodic corrugation of the edges[58] or periodic chain of holes,[61] the dispersion relation along one direction can be calculated for fixed coordinates in the plane orthogonal to the periodicity. For instance we can choose $y = y_0$ and $z = z_0$ and calculate dispersion relation along the x direction: $\widetilde{M}_{y_0,z_0}(f, k_x) = \mathcal{F}_{t,x}\left\{\hat{M}_i(t, x, y_0, z_0)\right\}$.

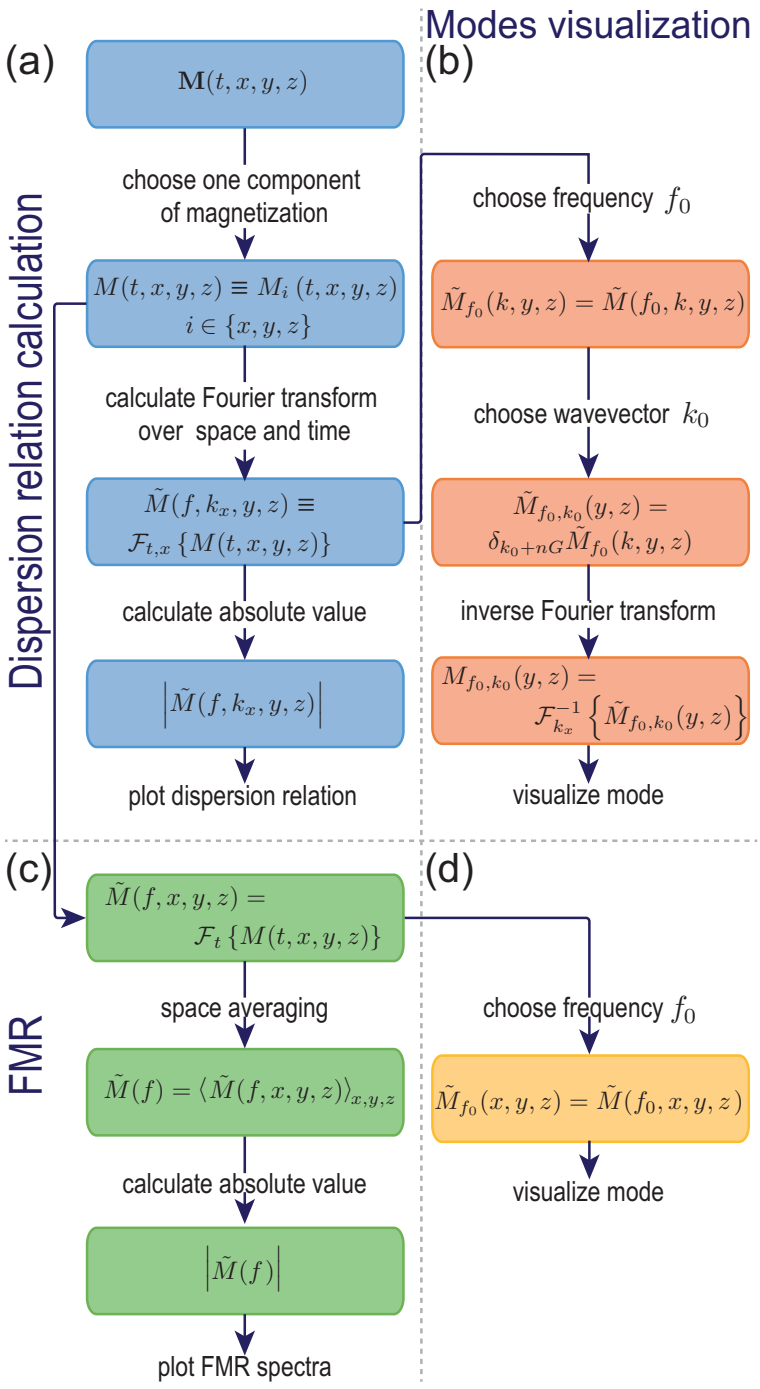

FIG. 7: The algorithm of post-processing of the micromagnetic simulations data in order to obtain: (a) dispersion relation, (b) visualization of the selected mode from the dispersion relation, which corresponds to the frequency f_0 and the wave vector k_0, (c) ferromagnetic resonance spectra, and (d) visualization of the SW mode corresponding to the resonance frequency f_0.

However, if it is essential to include the whole cross section into the analysis, in order to

obtain full dispersion, summation of the Fourier transforms corresponding for different slices of the (y, z) plane should be done: $\widetilde{M}(f, k_x) = \sum_{r,s} \mathcal{F}_{t,x} \left\{ \hat{M}_i(t, x, y_r, z_s) \right\}$, r and s index here the slices centered at positions $(y = y_r, z = z_s)$.

Result of FFT is complex ($\widetilde{M} \in \mathbb{C}$), and, therefore, to obtain dispersion relation the absolute value of the matrix $\left|\widetilde{M}(f, k_x)\right|$ needs to be visualized. In the case of higher dimensional MCs that process works analogously. Additionally, in order to improve quality and visibility of obtained dispersion relations various methods known from signal processing, in particular image processing can be used, i.e. to show less intense and eliminate spurious lines in dispersion.

4. Modes visualization

To identify SWs modes corresponding to the particular band, the distribution of the SW amplitude needs to be calculated. This can be done also from the matrix $\hat{\mathbf{M}}(t, x, y, z)$. The algorithm of such calculations is shown in Fig. 7(b). To simplify description, let us assume 1D MC (for higher dimensional MCs this process is similar) with dispersion relation in the form $\widetilde{M}_i(f, k_x, y_0, z_0)$. To visualize the SW excitation at frequency f_0 and wave vector $k_{x,0}$ we select from the matrix $\widetilde{M}_i(f, k_x, y_0, z_0)$ values corresponding only to the frequency f_0: $\widetilde{M}_{i,f_0}(k_x, y_0, z_0) = \widetilde{M}_i(f_0, k_x, y_0, z_0)$. In the next step, we further filter obtained matrix putting zeros to all values which correspond to k_x different from $k_{x,0} + nG_x$, where n is integer and G_x is reciprocal lattice vector along x:

$$\widetilde{M}_{i,f_0,k_{x,0}}(y_0, z_0) = \delta_{k_{x,0}+nG_x} \widetilde{M}_{i,f_0}(k_x, y_0, z_0) \tag{55}$$

The matrix $\widetilde{M}_{i,f_0,k_{x,0}}(y_0, z_0)$ consists of periodically appearing non-zero values, which correspond to wave-numbers $k_{x,0} + nG_x$. When we calculate inverse Fourier transform of $\widetilde{M}_{i,f_0,k_{x,0}}(y_0, z_0)$ we obtain complex matrix $M_{i,f_0,k_{x,0}}(x, y_0, z_0) = \mathcal{F}^{-1}_{k_x} \left\{ \widetilde{M}_{i,f_0,k_{x,0}}(y_0, z_0) \right\}$ which represents complex amplitude of the SW mode along the x-axis related to the $(f_0, k_{x,0})$ point in the dispersion relation.

5. Ferromagnetic resonance studies and visualization of the resonance modes

Computation of the SW dispersion relation is complex and time consuming. In many cases knowledge about full dispersion relation ($\omega(\mathbf{k})$) is not required, instead information

about ferromagnetic resonance frequencies, i. e. $\omega(k=0)$, and distribution of the standing SWs amplitude is sufficient, Fig. 7(c)].

Information about FMR can be derived by investigation magnetic response after applying spatially homogeneous magnetic field disturbing the static magnetization configuration. Due to homogeneity of the excitation it is possible to use PBCs, which allows to reduce significantly the size of the computational problem by simulation of only one unit cell. Similarly, as in previous case, we can apply the dynamic external field with similar time dependence $\mathbf{h}_{\mathrm{dyn}} \propto \mathrm{sinc}\,(2\pi f_{\mathrm{cut}} t)$. Results of simulations can be stored also in matrix $\hat{\mathbf{M}}(t,x,y,z)$. The FMR spectra can be calculated in two ways: i) as an absolute value of the Fourier transform of the averaged in space magnetization evolution: $\left|\mathcal{F}_t\left\{\left\langle \hat{M}_{x_i}(t,x,y,z)\right\rangle_{x,y,z}\right\}\right|$, or ii) as spatially averaged FFT over magnetization evolution in each simulated cell: $\left|\left\langle \mathcal{F}_t\left\{\hat{M}_{x_i}(t,x,y,z)\right\}\right\rangle_{x,y,z}\right|$. Where we have chosen x_i-th component of the magnetization vector and $\langle\cdots\rangle_{x,y,z}$ means the spatial average.

Having matrix $\widetilde{M}(f,x,y,z) = \mathcal{F}_t\left\{\hat{M}_{x_i}(t,x,y,z)\right\}$, spatial distribution of the amplitude of SW related to the resonance frequency f_0 can be reproduced [see, Fig. 7(d)]. For selected frequency f_0 we extract elements from the matrix in frequency domain, $\widetilde{M}_{x_i,f_0}(x,y,z) = \widetilde{M}_{x_i}(f_0,x,y,z)$ and obtain complex amplitude distribution in space corresponding to resonance frequency. Exemplary results of FMR spectra calculations with visualized modes' profiles corresponding to resonance frequencies are presented in Fig. 13.

6. Other utilizations of MS

In the previous part of this section we have presented MSs as a useful tool to obtain dispersion relation of SWs in MCs and to visualize SW excitations. However, MSs give much wider perspective for study other properties of MCs and more complex systems than ideal MCs.[62] This is investigation of the finite MCs, i.e. with the limited number of repetitions,[63] or MCs surrounded by other medias. MSs can be also used to study influence of defects on SWs' dynamics.[61] The influence of the boundary conditions at the interfaces between constituents of the MC on the dispersion relation can be also investigated with the use of MSs.[64,65] MSs are useful also for simulations of the transmission, reflection and scattering of SWs from the surface of the MC or defects. These investigations can lead to acquire additional information, especially important for applications. For instance, dependence of

the transmission on the frequency of SWs or influence of the MCs' surface on the transmission and coupling.

IV. MAGNONIC CRYSTALS

The magnonic band structures in 1D and 2D planar MCs presented in this section are calculated by numerical solution of the Eq. (35). The convergence of the obtained results is checked by numerical verification of the frequency changes with increasing number of plane waves used in Fourier expansions, N. When the frequency changes less than some set value we took this N for further the calculations.

A. Spin waves in planar magnonic crystals

The first experimental demonstration of the magnonic band structure formation and proof of existence of the magnonic band gaps in SW spectra of the bi-component 1D MC were done for Co and Py stripes.[66] The exemplary SW dispersion relations measured with BLS in MCs composed of Py/Co stripes of 150/250 nm and 250/250 nm width are shown in Fig. 19(a) and (b), respectively. Thus, for the explanation of the magnonic band structure in MCs we start from this type of 1D MCs, and subsequently we will present more complicated geometry, i.e., 2D planar MCs.

1. 1D magnonic crystals

The schematic picture of 1D planar MC under investigation is shown in Fig. 5. It consists of infinitely long stripes of two ferromagnetic materials (A and B) regularly arranged in the (y, z) plane. Materials are magnetized along the stripe axis, and SW propagation along the y axis is considered (this is the DE geometry). To understand formation of the magnonic band gaps, it is useful to remind the dispersion relation of SWs in homogeneous film with artificial periodicity introduced in Fig. 4, in the empty lattice model (ELM). This dispersion, limited to the first BZ, is shown also in Fig. 9(a), with artificial periodicity of $a = 500$ nm and in external magnetic field of magnitude of 0.1 T. The bands are degenerate at BZ boundary ($k = \pi/a$) and BZ center ($k = 0$). These degeneracies are removed, whenever contrast of

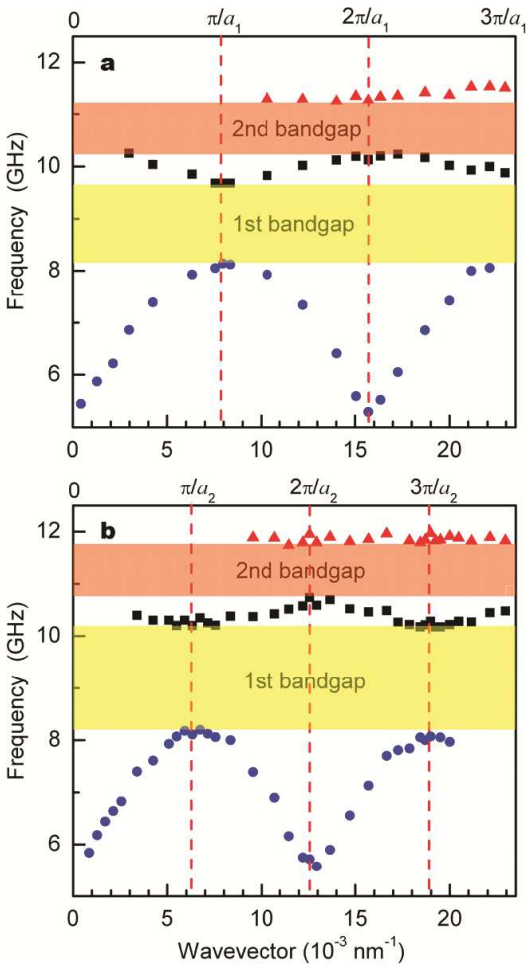

FIG. 8: Measured magnonic band structure in 1D MC composed of Co and Py stripes of (a) 150 nm and 250 nm thicknesses, respectively, and (b) 250 nm and 250 nm. The magnonic band gaps are marked by shaded rectangles. Reprinted with permission from Z. K. Wang, V. L. Zhang, H. S. Lim, C. Ng, M. H. Kuok, S. Jain, and A. O. Adeyeye, ACS Nano 4, 643 (2010). Copyright (2010) American Chemical Society.

any parameter relevant to magnetization dynamics will be introduced.

For instance, the change of the saturation magnetization and the exchange constant by 10% in material A is sufficient to split magnonic bands. In Fig. 9(b) the magnonic band structure of 1D MC composed of Py and an artificial material (with $M_{\mathrm{S}} = 0.9M_{\mathrm{S,Py}}$ and $A = 0.9A_{\mathrm{Py}}$) stripes shows magnonic band gaps between successive bands. There is magnonic band gap of 0.5 GHz width between first and second band. We assumed a filling fraction, i.e., the ratio of the A stripe width (a_{A} to the lattice constant, $ff = a_{\mathrm{A}}/a$), 0.5. Further increase of the magnetization contrast results in flattening of the bands and increasing band

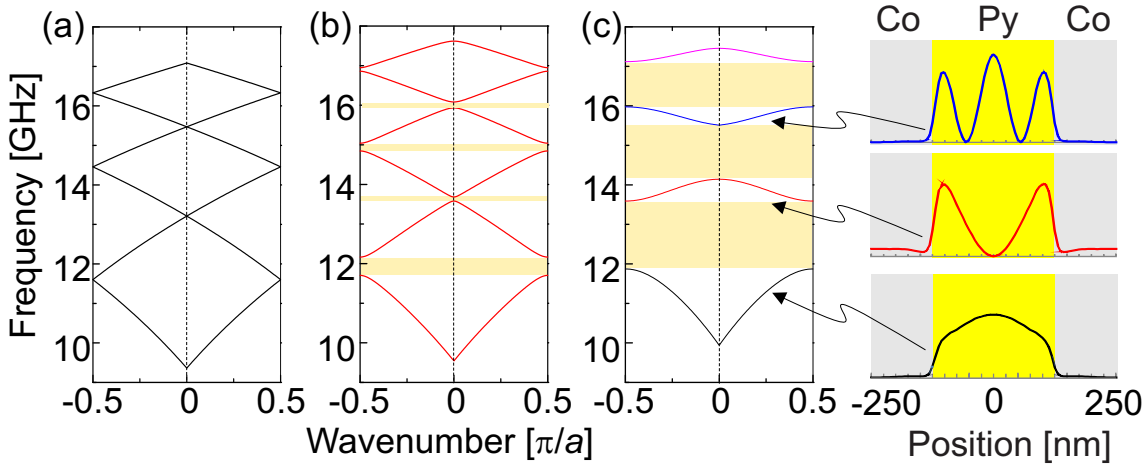

FIG. 9: (a), (b) and (c) Magnonic band structure in homogeneous Py film with artificial periodicity, in magnonic crystal (MC) composed of Py stripes and material with 10% increased M_S and A as compared to Py, and bi-component MC composed of Py and Co stripes, respectively. MCs are saturated by external magnetic field of 0.1 T, the filling fraction is 0.5. Magnonic band gaps are marked with shadow rectangles in (b) and (c). In (c) the amplitude of SW excitations from the three magnonic bands of lowest frequencies are also presented.

gap width. In Fig. 9(c) the SW band structure of the Co/Py MC is shown. At the same widths of Py and Co stripes, due to magnetization saturation and exchange constant of Py lower, than of Co, the magnonic bands at lowest frequencies are formed by standing SW excitations in Py stripes (see Fig. 9(c)).[67,68] In Co stripes there are present forced oscillations of the magnetization due to exchange coupling at interfaces. These amplitudes decay with increasing distance from the interface.

The band gap width and position in the frequency scale can be tailored by varying the structural parameters, such as filling fraction, lattice constant or film thickness. The magnonic band structure in dependence on these three parameters is shown in Fig. 10. The dependence on filling fraction [Fig. 10(a)] has two natural limits: $ff = 0$ the homogeneous Co film and $ff = 1$ the homogeneous Py film. At these values of ff the SW dispersion is continuous without band gaps, like in the empty lattice model in Fig. 9(a). The small change in filling fraction results in opening the band gaps. The gap between first and second band exists in the whole range of ff (excluding two limiting values) and the value of ff for the widest gap can be extracted. Other band gaps have non-monotonous change with ff and can be closed at intermediate values of ff.

The increase of the lattice constant results in shift of the BZ boundary to smaller wavenumbers. It means that the first band will end at lower frequencies. The low frequency cut-off of the magnonic spectra (the FMR frequency) is almost independent on the change of a, pointing at the unpinned magnetization dynamics at the Py/Co interfaces. These contradictory changes of the first magnonic band edges result in significant increase of the width of the first magnonic band with decreasing a. Indeed, such dependence is observed in Fig. 10(b), where magnonic band structure of the Co/Py MCs projected on the frequency scale is plotted in dependence on a, for fixed $ff = 0.5$ and $d = 20$ nm.

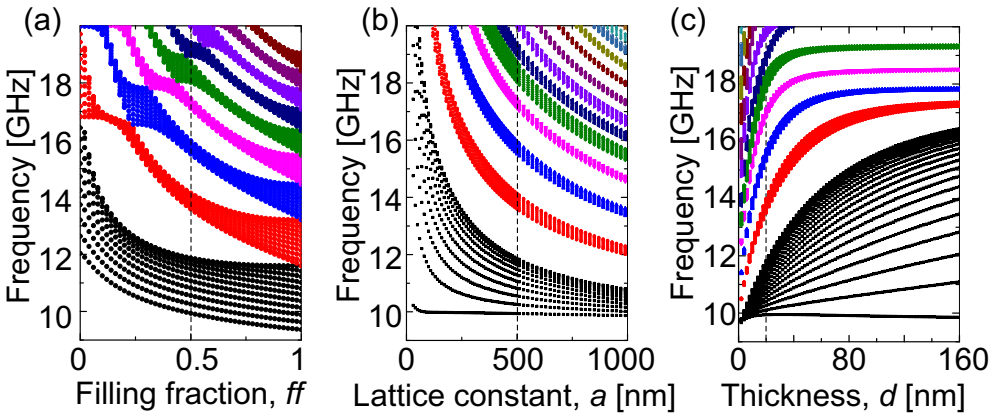

FIG. 10: Magnonic band structure calculated with PWM in Co/Py bi-component MC in dependence on (a) filling fraction, (b) lattice constant and (c) thickness of the MC. In (a) the lattice constant and thickness are fixed to 500 nm and 20 nm, respectively. In (b) the filling fraction is 0.5 and the thickness is 20 nm. (c) The lattice constant and filling fraction are 500 nm and 0.5, respectively. In all plots external magnetic field of 0.1 T is parallel to stripes. In all figures the vertical dashed line points at the band structure of the same MC, i.e, MC with the band structure presented in Fig. 9(c).

Dependence of the magnonic band structure on the MC's thickness is shown in Fig. 10(c) for Py/Co MC with fixed lattice constant (500 nm) and filling fraction (0.5). We can see, that the influence of d is substantial for the width of the first band. This dependence has the same origin as the dependence of the dispersion relation of the DE wave on the thickness in homogeneous film. It is, the increase of the film thickness pull up the group velocity of SWs to higher values in the long wavelengths. The higher bands increases frequency with increasing thickness, but they saturate already at relatively small d. For larger d the bands are narrow (apart from the first band), what points at weak coupling between SW

excitations in neighbor stripes. The excitations from these bands have nodal points across Py width, making the dynamical magnetostatic field, which is responsible for the coupling, weak. In calculations we have neglected the variation of the dynamical magnetization across the MC thickness, thus the standing SW resonances are excluded from this consideration.

The other types of MCs are these composed of separated ferromagnetic stripes. In this case only dipole interaction are responsible for formation of the magnonic band structure. Thus the size and shape of stripes and separation between them steer collective SWs dynamics.[69] The possibility for control of the magnetization alignment in the arrays of stripes (ferromagnetic or antiferromagnetic) has allowed to demonstrate the reprogrammable magnonic band structure in MCs.[70–74]

The periodicity in magnonic systems can be introduced also in other ways. For instance, the periodic modulation of the external magnetic field applied to homogeneous film is sufficient to create magnonic bands and band gaps.[75,76] Also an array of groves etched on the surface of the film, periodic magnetic anisotropy field induced from inhomogeneous substrate, or regular array of non-magnetic metallic stripes on homogeneous film are also sufficient for formation of the magnonic band structure. Each type of periodicity has its own specificity,[77] which can be exploited for various applications.

2. 2D magnonic crystals

Among the plane 2D MCs we can distinguish three main types of MCs. These are arrays of dots, antidot lattices (ADL) and bi-component MCs (BMC), as shown schematically in Fig. 11 (a), (b) and (c), respectively. The former is composed of a regular array of thin ferromagnetic dots (material A), the second is a negative of the former, i.e., it is created by an array of holes in thin ferromagnetic film of the material B. The last group can be regarded as a superposition of both, i.e., the ADL with holes filled with ferromagnetic material different from the material of the ADL. Those three groups present distinct features in the SW propagation, which we will discus in this section.

The collective dynamics of the magnetization in the array of dots is solely due to dipole coupling between excitations of the dot. The SW excitations are also influenced by static demagnetizing field (including a stray magnetic field from the array) resulting in a change of profile of the internal magnetic field (see Fig. 12(a)) and change of the magnetization

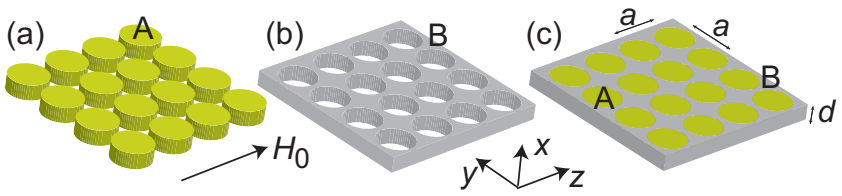

FIG. 11: Two dimensional planar MCs: (a) the array of ferromagnetic dots made from material A, (b) antidot lattice of material B, and (c) the bi-component MC composed of materials A (material of the dots) and B (host material). All MCs have square lattice with lattice constant a and thickness d.

configuration. In the case of weak coupling (large separation between dots with respect to their thickness and magnetization), the magnonic spectra consists of flat bands with SW excitations corresponding to the eigenmodes of the isolated dot. These are edge modes (EMs), fundamental mode (FM) and modes with the nodal lines along (BA) and/or perpendicular (DE) to the direction of the external magnetic field. They can have measurable intensity (see FMR spectra in Fig. 13(a)) and are visualized in Fig. 13(b) and (c) for the array of weakly coupled Py dots due to their significant separation. The EM amplitude is concentrated near the ends of the dot in the wells of the internal magnetic field formed by the demagnetizing field (Fig. 12(a)). The FM has no phase oscillations and the maximum of the amplitude concentrated in the middle part of the dot.

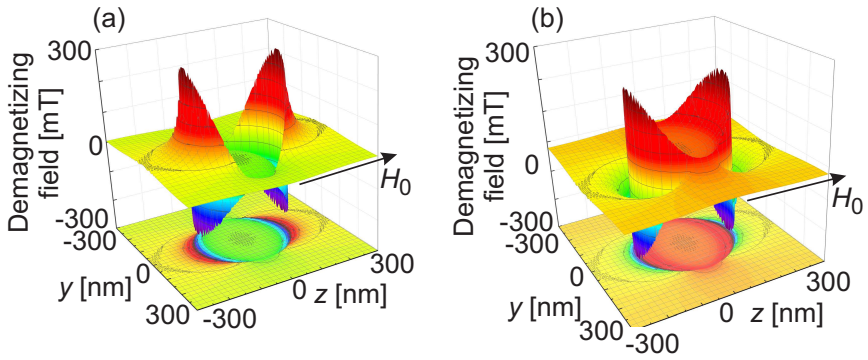

FIG. 12: The demagnetizing field calculated from the Eq. (47) (with the minus sign) in (a) array of Py dots (radius 150 nm) and (b) in the antidots lattice (ADL) (radius of holes 150 nm). In both cases the thickness of Py is 20 nm, period of the square lattice 600 nm and saturation along the z axis.

When the coupling between dots increases, the levels of eigenmodes split into the bands.

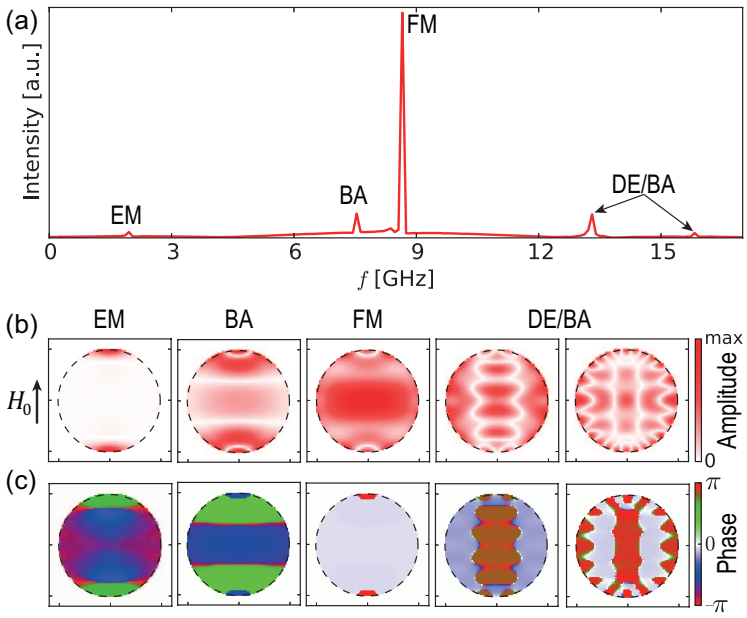

FIG. 13: (a) Ferromagnetic resonance (FMR) spectra, (b) amplitude and (c) phase distribution of the SW excitations in the array of the Py dots array (radius 150 nm, lattice constant 600 nm, thickness 20 nm and external magnetic field $\mu_0 H_0 = 0.1$ T). The modes in (b) and (c) are ordered with increasing frequency from the left to right: edge mode (EM), mode with nodal lines along the direction of the external magnetic field (BA), fundamental mode (FM), and high frequency modes with nodal lines along and perpendicular to the magnetic field (DE/BA). The results of the micromagnetic simulations.

However, the dynamic dipole interaction between dots is effective only for selective eigenmodes. From these types of modes collective excitation of the array can be formed.[36] In Fig. 14 the dispersion relation of SWs in the array of Py circular dots (diameter 600 nm, thickness 50 nm and lattice constant 655 nm) measured with Brillouin light scattering (solid dots) and calculated with dynamical matrix method (lines) are shown.[78] The bands connected with the fundamental (thick solid line) and low order BA magnetostatic mode type show valuable dispersion (i.e. nonzero slope of the band). The other types of the excitations (edge modes, bulk modes with high quantization or perpendicular standing spin waves (PSSWs)) are dispersionless.

In ADL, the low frequency part of the SW spectra is determined by profile of the inhomogeneous static demagnetizing field created by magnetic surface charges at edges of the holes, which has reverse shape as compared to the array of dots (compare Fig. 12(a) and (b)). Due

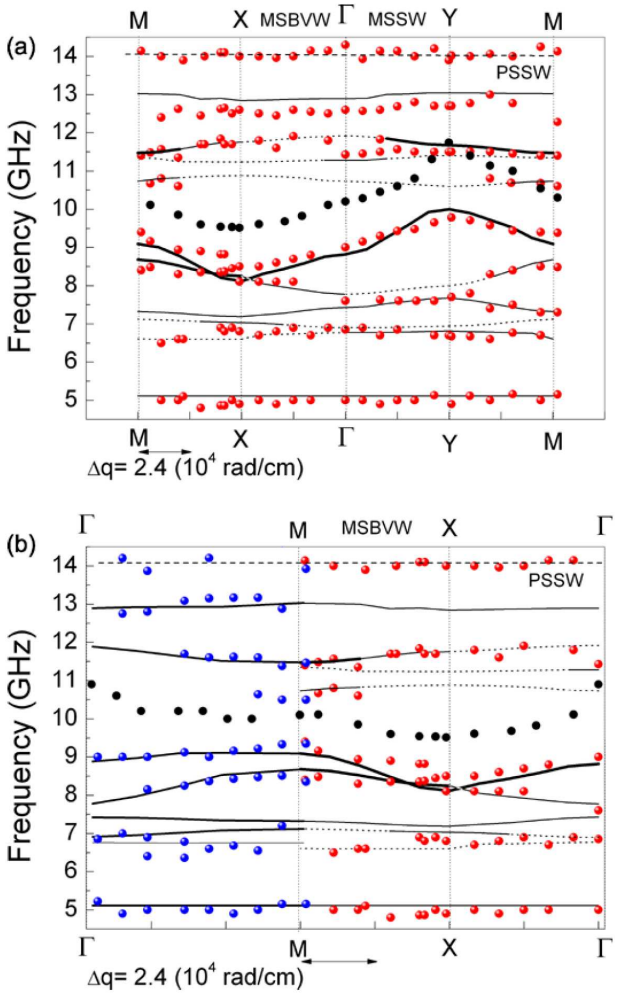

FIG. 14: Measured (full circles) and calculated (lines) magnonic band structure for the 2D array of NiFe disks plotted along two different paths of the first BZ (ΓYMX in panel (a) and ΓMX in panel (b), respectively). Full black circles are the measured frequency for the continuous (unpatterned) NiFe film of the same thickness. [Figure taken from G. Gubbiotti, S. Tacchi, M. Madami, G. Carlotti, R. Zivieri, F. Montoncello, F. Nizzoli, and L. Giovannini, *Spin Wave Band Structure in Two-Dimensional Magnonic Crystals* in S.O. Demokritov, A.N. Slavin (eds.), *Magnonics*, Topics in Applied Physics **125**. Copyright Springer-Verlag Berlin Heidelberg 2013. With kind permission from Springer Science and Business Media.]

to this field, wells of the internal magnetic field form close to the holes and magnetization dynamics can concentrate amplitude in these areas. Indeed in ADL, EM localized at the edges of the holes and SWs concentrated in channels between holes were found (Fig. 15).

The transition of the SWs (EM and fundamental mode) from quantized to propagative can be controlled by separation between antidots but what is more interesting also in the same structure by change of the magnetic field direction. In addition to the demagnetizing effects, the quantization of the SW excitations modify the spectra. This effect dominates for exchange SWs, i.e., at high frequencies or when the lattice constant is small.[61,79]

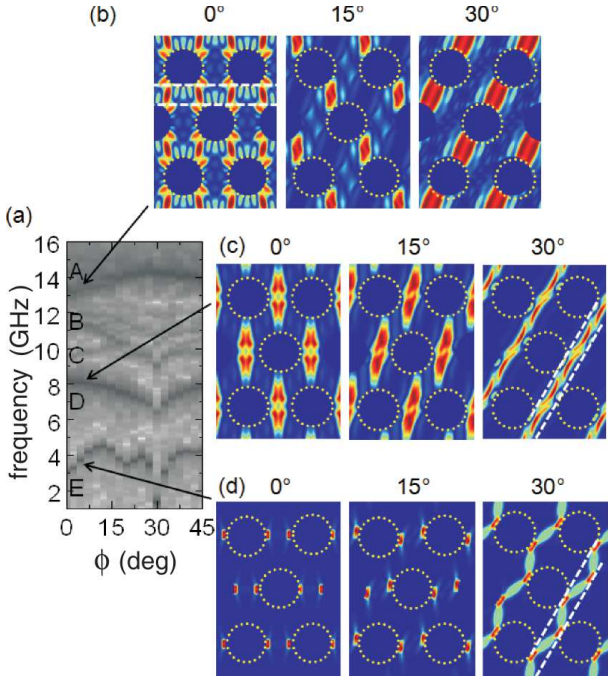

FIG. 15: (a) SW spectra at zero weve number as a function of the angle of the external magnetic field in ADL made from 30 nm thick Py film with rhombic array of holes (of 250 nm diameter). Amplitudes of SWs from bands A, D and C marked in (a) for 0, 15 and 30 degree. Dotted lines mark position of the holes. Reprinted from Ref. [49]. Copyright (2012) by the American Physical Society.

In BMC the inhomogeneous demagnetizing field is still present, however its amplitude depends on the difference between magnetization of the constituent materials. Thus, the influence of the demagnetizing field on SW dynamics is weaker than in ADL. The BMC composed of Co circular dots embedded in Py ($Ni_{80}Fe_{20}$) matrix were investigated experimentally.[80,81] The BLS measurements showed the existence of the two types of low frequency SW excitations concentrated in regions perpendicular to the external magnetic field, one containing Co dots and second in Py matrix between the Co dots.[82]

For demonstration the principle properties of magnonic band structure in 2D BMCs we

consider MCs composed of square lattice of circular Co dots of radius $R = 155$ nm (material A) embedded in Py (host material B) as shown schematically in Fig. 6(a). We assume lattice constant $a = 600$ nm and thickness 20 nm. The first BZ has a square shape covering wave vectors with in-plane components k_y and k_z between $-\pi/a$ to π/a as shown in Fig. 6(b), at the first BZ border $k \approx 5 \times 10^6$ m^{-1}. The magnetic field is in the film plane along the z axis. The structure and its parameters are fixed to values used in Ref. [81].

We start with the discussion of the model of homogeneous ferromagnetic film with an artificial periodicity, i.e., the ELM. The results of the PWM calculations for 20 nm thick film with a square lattice artificial periodicity and averaged values of magnetic parameters (of Co and Py) are shown in figure 16(d). There is a dense spectrum of magnonic bands, which is a direct consequence of the periodicity. The analytical dispersion relation of SWs in a homogeneous thin film is marked by bold dashed line (red online). We see a perfect coincidence of the analytical and numerical results.

We can qualitatively explain that spectra based on properties of the Bloch's theorem (Sec. III A). The discrete translational symmetry in real space introduces the periodicity of the dispersion relations $f(\mathbf{k}) = f(\mathbf{k} + \mathbf{G})$. In the center of the BZ ($k = 0$) additional solutions (frequencies 2 – 9) occur as compared to the single solution (frequency 1) in the homogeneous film. These solutions are exactly the same as for spin waves with wave vectors equal to the respective reciprocal lattice vectors. In the case of the ferromagnetic film considered here, SWs with wave vectors $\mathbf{k} = \mathbf{G}_{01}$, $\mathbf{G}_{02}$, $\mathbf{G}_{03}$ and $\mathbf{G}_{04}$ have frequencies below 7.57 GHz (the indexes for reciprocal lattice vectors refer to centers of the successive BZs: $\mathbf{G}_{n,m} = 2\pi/a\,(n, m)$, see Fig. 16 (a)). It means that these frequencies are below the frequency of the DE mode at the first BZ boundary [7.57 GHz, right edge of Fig. 16(b)]. The new mode frequencies appear at the BZ center (frequencies 2 - 9) once the periodicity is introduced, as it is schematically shown in Fig. 16 (b) by arrows. The same will happen for other wave vectors with $k \neq 0$ in the first BZ.

Because in ELM the periodicity is artificial, the eigenvector solutions should be consistent with the plane waves, being solutions of the homogeneous film. The profiles of the SW modes calculated within the ELM in the BZ center are shown in Fig. 16(c) and they are just the same as plane wave solutions of the homogeneous thin film with wave vectors being equal to the respective reciprocal lattice vectors. Not shown in Fig. 16 (c) is profile of the mode 1 because it is a uniform excitation. The pairwise degeneracy of the modes 2 and 3, 4 and

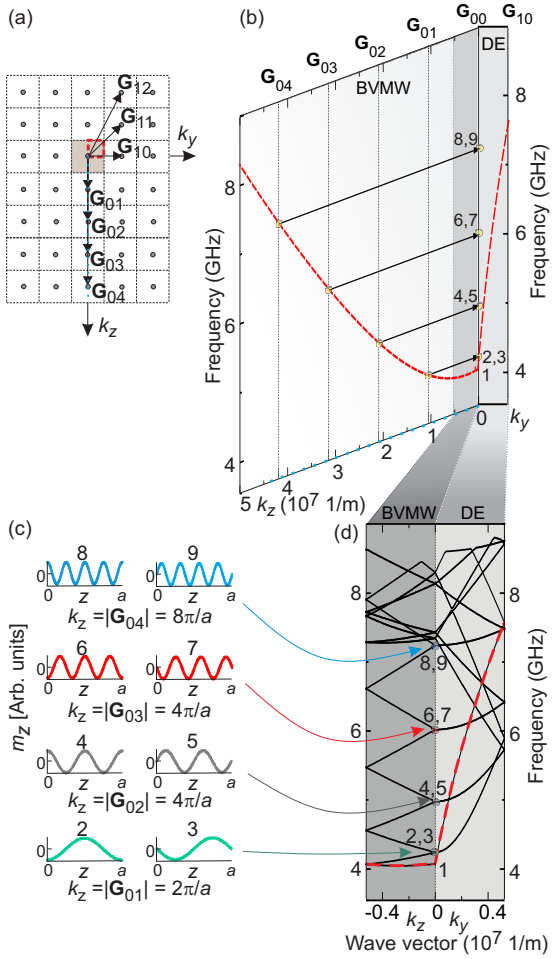

FIG. 16: (a) Reciprocal space with a few reciprocal lattices vectors ($\mathbf{G}_{ij}$) for the 2D MC with a square lattice. The gray-shaded area marks the first BZ. (b) Dispersion relation (dashed lines) of SWs in a homogeneous ferromagnetic thin film with in-plane magnetization and external magnetic field ($\mu_0 H_0 = 0.02$ T). The dispersion is shown along the k_z and k_y direction, i.e., in BVMW and DE geometry, respectively. Vertical dotted lines show positions of the $\mathbf{G}_{ij}$ introduced by periodicity. The gray-shaded area marks the first BZ that would follow from a periodicity of 600 nm. (c) The spin-precessional amplitudes of SWs at the center of the BZ as derived from the ELM (modes 2 to 9). The respective value of the wave vector is written below each mode. (d) Magnonic band structure in the first BZ for the homogeneous film with the artificial periodicity introduced (the lattice constant $a = 600$ nm), i.e., the empty lattice model (ELM). The part of the dispersion from (a) is marked by a bold dashed line (red online). The low-frequency branches along k_z are formed directly by shifts (back-folding) of the SW dispersion relation from higher-order BZs by respective reciprocal lattice vectors. The frequencies in the BZ center ($k = 0$) are obtained by shifts according to the arrows shown in (a).

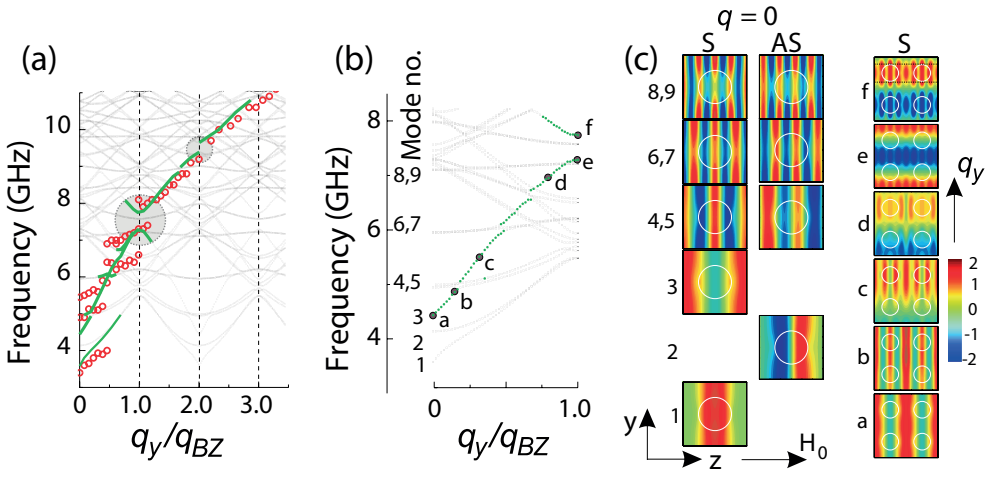

FIG. 17: (a) Magnonic band structure of a 2D bi-component MC consisting of Co dots in Py with $a = 600$ nm calculated along different directions of the first BZ of Fig. 6 (b). The sample is saturated along the z-axis by the static external magnetic field $\mu_0 H_0 = 0.02$ T. The bold dashed line (green online) marks the DE-like mode in the first BZ. (b) Modulus of the spin-precessional amplitude for low frequency modes with wave vectors from the center of the BZ (Γ point). The numbers 1 to 9 in (a) and (b) indicate the mode number. In (b) the SW profiles are grouped into symmetric (S) and antisymmetric (AS) modes with respect to a line parallel to the y-axis and crossing the Co dots in the middle. (Note: the wave vector in this figure is indicated by q.) Reprinted from Ref. [81]. Copyright (2012) by the American Physical Society.

5, 6 and 7, 8 and 9, seen in Fig. 16 (d) is a direct consequence of the artificial periodicity. The profiles of these sets of degenerate modes have the same shape but are shifted by $a/4$ along the z-axis, thus in the homogeneous film their energies are degenerate.

The magnonic band structure calculated along the path Z-Γ-Y-M-Z of the first BZ [Fig. 6 (b)] for a 2D BMC composed of Co dots in Py is shown in Fig. 17. The MC is saturated in the periodicity plane along the z-axis by an external magnetic field $\mu_0 H_0 = 0.02$ T. According with expectations from ELM (Fig. 16(d)), the magnonic band structure in Fig. 17 is composed of many bands. We can point at the obvious similarity between the magnonic band structure of BMC shown in Fig. 17(a) and the SW dispersion calculated in the ELM (Fig. 16 (d)), but there are also discrepancies. We distinguish four main differences:

i. *The low frequency of the first mode in the bi-component MC.* This is an effect of the static demagnetizing field which decreases the effective magnetic field in Co at

the interfaces with Py (due to higher magnetization in Co than in Py) and creates potential wells for SWs, resulting in mode channeling confirmed by micro-focused BLS measurements.[80]

ii. *The larger splitting of the bands 2 and 3 and small splittings between the bands 4 and 5, 6 and 7, 8 and 9.* Near the Γ point, the spin wave modes 1 and 3 concentrate their maxima in two complementary channels parallel to the y-axis comprising of the Co dots and in between them, respectively (Fig. 17(b)). In comparison to the spectrum of the ELM (Fig. 16 (d)), the dispersive branch of the mode 3 in the bi-component MC is shifted to higher frequencies near the Γ point with respect to mode 2. This effect is also due to the inhomogeneous demagnetizing field not considered in the ELM.

The dispersions $f(k)$ of the modes 4 to 9 in the spectrum of both the BMC and ELM are very similar. These modes in the center of the BZ are directly related to the BVMWs of the homogeneous film folded back into the first BZ due to periodicity. The profiles of the plane waves from the ELM (Fig. 16(c)) and amplitudes of modes in the bi-component MC along the z-axis (Fig. 17(b)) are closely related to each other. In the unit-cell center (i.e., in the Co dots) there are maxima of the spin-precessional amplitudes for symmetric modes (modes 4, 6 and 8) and nodal lines for antisymmetric modes (5, 7 and 9). These differences in the position of amplitude maxima are responsible for the band splittings at the BZ boundary and center. The splittings between bands in the bi-component MC decrease with increasing mode number.

iii. *The crossing and anti-crossing between DE mode and other SW excitations in the BMC.* We have already shown that with increasing wave vector component k_{y}, the DE mode (marked by a bold dashed line (green online) in Fig. 17(b)) crosses other bands in the ELM (Fig. 16(d)). Because folding to the first BZ is due to the artificial periodicity in the ELM, interaction between modes is absent. But in the BMC the DE-like mode interacts with other modes.

iv. *Magnonic band splitting at the BZ boundary or center.* This splitting results from the destructive interference of Bragg reflected DE-like SWs at the BZ boundary.[81] The value of this band splitting at the first BZ border can be estimated analytically based on the PWM formulas.

The DE-like wave can be considered as 1D wave which propagates along the y axis. Then, limiting the Fourier expansions (34) to the two dominating plane waves, i.e., with coefficients $\mathbf{m}_{\mathbf{k}_{\mathrm{BZ}}}(\mathbf{G}_0 = 0)$ and $\mathbf{m}_{\mathbf{k}_{\mathrm{BZ}}}(\mathbf{G}_{10} = [\frac{2\pi}{a}, 0])$, the frequencies of the first (f_-) and second (f_+) DE-like bands at the BZ boundary ($\mathbf{k}_{\mathrm{BZ}} = [\frac{\pi}{a}, 0]$), at the points e and f in Fig. 17(d), respectively, can be expressed as:

$$f_\pm = \frac{\gamma\mu_0}{2\pi}\sqrt{H_0 + C_{k_{\mathrm{BZ}}}(M_{\mathrm{S}}(0) \mp M_{\mathrm{S}}(G_{10}))} \times\sqrt{H_0 + (1 - C_{k_{\mathrm{BZ}}})(M_{\mathrm{S}}(0) \mp M_{\mathrm{S}}(G_{10}))}, \tag{56}$$

where $C_k = \frac{1-\mathrm{e}^{-|k|d}}{2}$ and $M_{\mathrm{S}}(G)$ is calculated from Eq. (33). From this equation, we find that the width of the band gap increases almost linearly with the magnetic contrast, i.e., with $M_{\mathrm{S,Co}}$ – $M_{\mathrm{S,Py}}$. This property was confirmed experimentally.[81]

For SWs in thin films with out-of-plane magnetization the isofrequency contours are isotropic, mimicking the case of electromagnetic waves in an isotropic dielectric medium.[33,83] Moreover, in the dipole dominating part of the spectra ω is a linear function of k (see bottom part of Fig. 3(f)). The magnonic band structure of homogeneous Py film magnetized perpendicular to its plane (by the external magnetic field 1.2 T) with the artificial periodicity $a = 600$ nm (the ELM) is shown in Fig. 18(a). We can see the linear dispersion relation of spin waves and degeneracy of the first and the second magnonic band at the first BZ boundary marked by dashed line. As compared to the geometry with the in-plane magnetic field, the frequency at the BZ border is similar for different directions of $\mathbf{k}$ (it belongs to the range between 6.6 and 6.8 GHz). This means, that the magnonic band gap shall be more easy to open in FVMW geometry, than in BVMW-DE geometry.

In Fig. 18 (b) we show the magnonic band structure of the MC composed of square lattice of Co dots embedded in Py thin film (10 nm thick). Both materials are magnetized perpendicular to the film plain. Due to the narrow bands and large magnonic band gaps we split the figure into two separate plots showing first band (bottom plot) and second with third band (top plot). The narrow bands point at localized character of the spin wave excitations, which is confirmed by spatial distribution of the spin wave amplitude shown in Fig. 18(c). In all three bands the spin waves concentrate in Co dots and their frequencies are close to the normal excitations of the Co dot, slightly broadened by the interaction in the array. This strong concentration of the spin wave amplitude in Co is the result of static demagnetizing field which is much larger in Co than in Py.

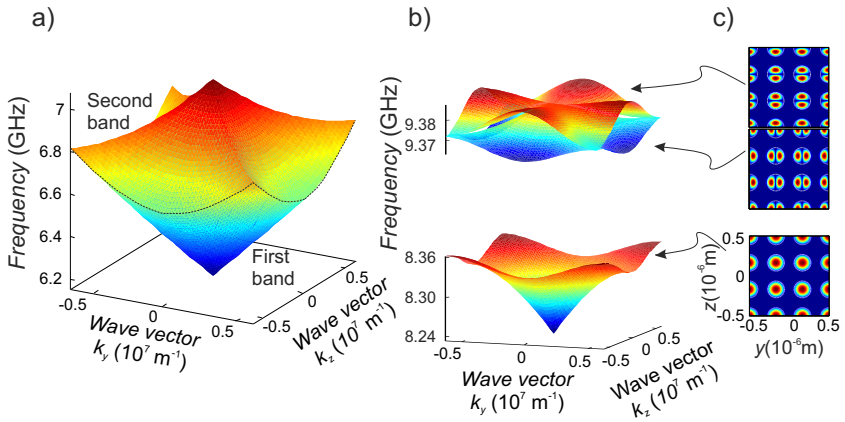

FIG. 18: (a) Magnonic band structure of a homogeneous Py film magnetized perpendicular to the film plane with an artificial periodicity of the square lattice. External magnetic field $\mu_0 H_0 = 1.2$ T, the lattice constant $a = 600$ nm and film thickness of 10 nm was assumed. (b) Magnonic band structure of bi-component magnonic crystal (Co dots of 155 nm radius in Py matrix) in FVMW geometry with perpendicular magnetic field 1.5 T. The different frequency scale is assumed for the first and second with third band. (c) Modulus of the amplitude of the dynamical component of magnetization vector for spin wave modes from the center of the BZ.

3. Exchange spin waves in 2D MCs

Molding the flow of exchange SWs can be realized in MCs with sufficiently small lattice constant. Decrease of the lattice constant results in the shift of the BZ boundary toward large wave vectors, up to the value where at BZ boundary the exchange dominates over the dipole interactions. In that case magnonic band structure is formed from a parabolic dispersion relation in ELM.

The magnonic band structure in the ADL made from thin Py film (3 nm thick) with square holes (the edge length 12 nm) and the lattice constant of 30 nm is shown in Fig. 19(a). In this figure, the results of the PWM are superimposed with the results of micromagnetic simulations, with good agreement between both methods. The wide magnonic band gap is opened between the first and the second band. As expected, the dispersion relation is parabolic around the Γ point (around the BZ center). However, still some anisotropy resulting from the magnetostatic interactions is present, which can be seen in isofrequency contours, which show elliptical deformation, see for instance Fig. 19(b) and contour for $f = 63$ GHz.

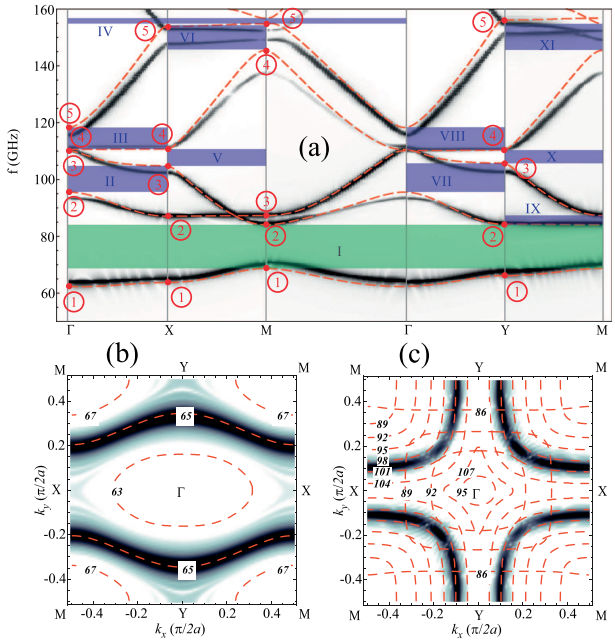

FIG. 19: (a) Magnonic band structure in ADL with square lattice of the square holes in Py film. The solid (red dashed) lines shows the results of the micromagnetic simulations and PWM calculations, respectively. The full magnonic band gap is marked by green rectangle. (b) and (c) Isofrequency lines on the k_y and k_z wave vector plane. Reprinted with permission from [60]. Copyright [2014], AIP Publishing LLC.

Also in BMC the decrease of the dipole interaction results in significant changes of the magnonic band structure. The PWM results for BMC with dominated exchange interactions are shown in Fig. 20. We chose square lattice (lattice constant $a = 50$ nm) of the Ni dots as the material of inclusions and Fe as a material of the host, and the film thickness 10 nm. We assume external magnetic field 50 mT in the MC plane. The contribution of the dipole interactions is still taken into account in calculations. The flat band (with a little negative slope near the Γ point) along the direction of the magnetic field ($\Gamma \rightarrow$ X) is a signature of the BVMW geometry, while the linear slope along orthogonal direction ($\Gamma \rightarrow$ X') is due to DE geometry. The anisotropy in the dispersion is still present at the BZ boundary (at X the frequency is 14 GHz while at X' it is 12 GHz) but the full magnonic band gap is opened in this case, as opposed to Fig. 17(a). This gap is an indirect, as the maximum of the first band is at the M point and minimum of the second band is at X. As expected, due to the lower FMR frequency of Ni as compared to Fe, the modes from the first two bands have an amplitude concentrated in Ni. This makes the magnonic bands (and magnonic gap) robust

on the distortions of the shape of inclusions.

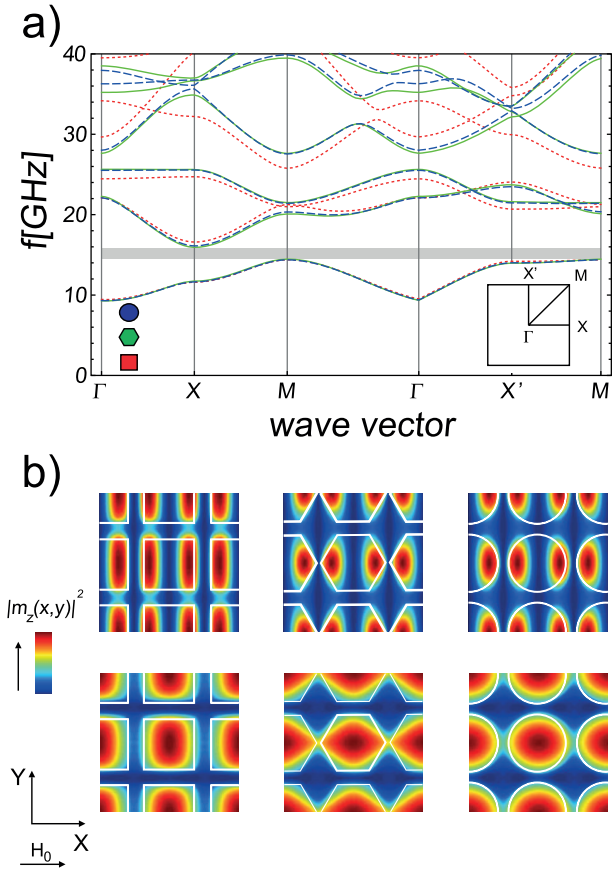

FIG. 20: (a) Spin wave spectrum for a square lattice of square, hexagonal and circular (red, green and blue lines) Ni inclusions in an Fe host with the small lattice constant $a = 50$ nm. The assumed values of the structural parameters are: filling fraction $ff = 0.55$ and slab thickness $d = 10$ nm. An external magnetic field $\mu_0 H_0 = 50$ mT is applied in the film plane along the x-axis. (b) Spatial distribution of amplitude of the z-component of the dynamic magnetization for the first (bottom row) and second (top row) magnonic band in the vicinity of the point Γ. Reprinted with permission from [84]. Copyright [2012], AIP Publishing LLC.

To investigate the impact of the lattice symmetry and the inclusion shape on the spin wave spectrum the circular, square and hexagonal inclusions arranged in a square lattice and a triangular one were considered with fixed filling fraction (see Fig. 20).[84] It was found, that the shape of inclusions does not play significant role in the range of small lattice constant values. However, the symmetry of the lattice is of much importance for the spectrum. In the spectrum of the MC with the triangular lattice the band gap is significantly wider,

than in the square lattice.[84] The same conclusions were obtained for photonic crystals. The symmetry reduction by rotating inclusions of non-circular shape or additional scatterer in the unit cell in 2D MC gives additional possibility for tuning magnonic band gaps.[85,86]

B. Spin waves in 3D magnonic crystals

The extension of the PWM to calculation of the magnonic band structure in 3D MCs was developed in Refs. [87–90]. In these papers systematic study of the effect of many factors on the magnonic band structure were presented. The considered factors include structural parameters (filling fraction, lattice constant, ellipsoidal deformation of the scattering centers) and magnetic properties of the constituent materials (contrast of saturation magnetization and exchange constant).

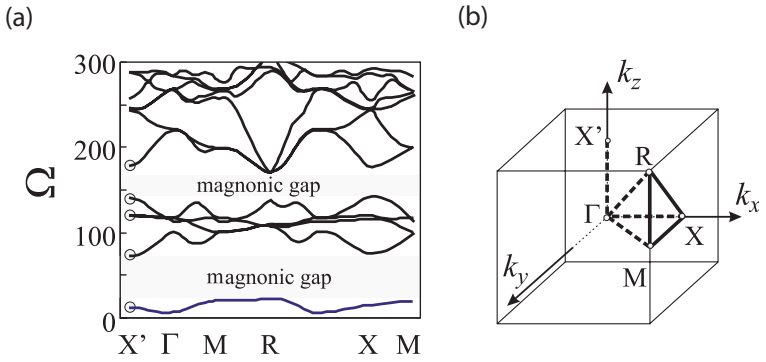

FIG. 21: (a) The magnonic band structure of simple cubic magnonic crystal with lattice constant 100 $\mathring{A}$. The MC is composed of Fe spheres (radius 26.28 $\mathring{A}$) embedded in YIG. The band structure is plotted along the path in the first BZ shown in (b). Reprinted from Ref. [87]. Copyright (2008) by the American Physical Society.

The magnonic band structure of the simple cubic (sc) lattice composed of Fe spheres in the YIG matrix is shown in Fig. 21(a). The calculations are performed along irreducible part of the first BZ shown in Fig. 21(b). Apart of sc lattice also body-centered cubic (bcc), face-centered cubic (fcc), and simple hexagonal (sh) crystallographic structure were investigated.[87–90] Both magnetic contrasts, i.e. the saturation magnetization and the exchange constant contrast, were shown to play an important role in the opening of magnonic gaps. A saturation magnetization contrast above a certain critical level provides a sufficient condition for magnonic gaps to open (even if the values of the exchange constant in the

constituent materials are equal); the critical value of saturation magnetization strongly depends on the lattice type. The exchange contrast has a signicant effect on the gap width, but needs to be very large to induce the opening of magnonic band gaps in the absence of magnetization contrast. As demonstrated in Ref. [87], an important role in the creation of magnonic band gaps is played by the crystallographic structure. The best conditions for the occurrence of magnonic band gaps are offered by the fcc lattice. Moreover, the results of these calculations indicate that the gap width depends on the shape of the scattering centers; in the fcc and bcc structures the largest band gaps are observed for scattering centers with a shape close to a sphere. The important role of the lattice constant is demonstrated in cubic magnonic structures, in which, for lattice constants greater than the exchange length in the matrix material, the dipole interactions gain in importance, which results in a substantial reduction of the gap width.

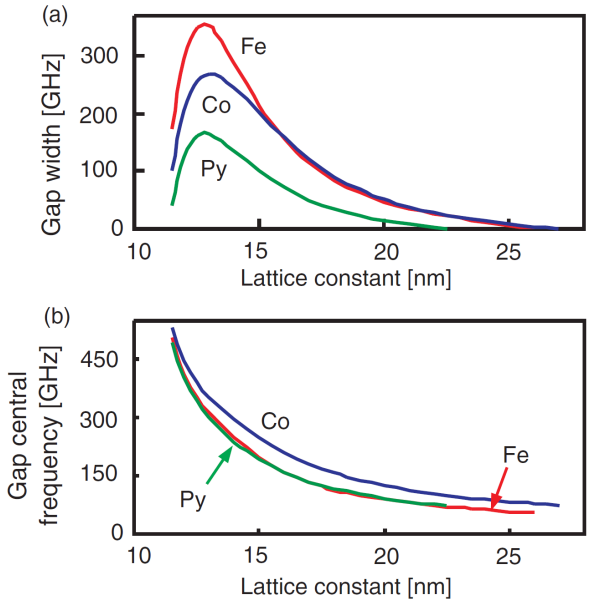

FIG. 22: (a) The magnonic band gap width and (b) the frequency of its central point in magnetoferritin based 3D MC of fcc structure with the host material being Fe (red line), Co (blue line) and Py (green line). Reprinted from Ref. [90]. Copyright (2012) by the American Physical Society.

However, fabrication of the bi-component 3D MCs is big challenge, especially if the lattice constant is in the nanometer range. The promissing approach is a fabrication based on self-assembling magnetic nanoparticles,[91] or exploit existing 3D dielectric structures.[92] The usage of cage-like proteins to grow magnetic NPs, e.g., magnetoferritin (mFT), a biomimetic

nanoparticles based on a ferritin, has many advantages: high level of homogeneity, variety of the sizes and properties of protein cages, diversity in physical or chemical functionality of protein shells, which allows to control the self-assembly process without modifying the NPs obtained inside the protein cages. Moreover, mFT NPs can be filled with numerous magnetic materials resulting in different magnetic properties of the NPs.[93] The protein crystallization technique was used to crystallize mFT NPs, allows to produce highly ordered 3D structures up to about 0.4 mm in size.[94,95] Obtained mFT crystals have high quality fcc structure and the lattice constant about 18.5 nm. Moreover, it was shown theoretically that dried mFT crystals have the crystallographic structure and the lattice constant almost optimized for the occurrence of a complete magnonic band gap, whenever the proteins will be replaced by ferromagnetic material, see Fig. 22.[90]

V. APPLICATIONS

Magnonics is a young field of nanoscience and technology dedicated to exploration of the coherent magnetization dynamics in nanoscale.[96–99] Its one of the main objectives is to exploit the spin wave dynamics for technological applications, including usage of spin waves for carrying and manipulating information.[23] The advantages of magnonics over electronics and photonics include low energy consumption and fast operation rates as compared to electronic devices,[100] and possible integration with standard CMOS technology, at levels impossible to achieve with electromagnetic waves.[101] Besides that, processing with spin waves allows easy tunability by the external magnetic field,[25] low energy costs tunability by electric field or stress when combined with magnetoelectric or magnetostrictive materials.[102,103] It can be influenced also by electric current[104,105] and allows for magnetic momentum transfer without charge transport, thus magnon spintronics[106,107] gives a chance for competing with electronics and spintronics which is based on charge transport. Moreover, magnetic structures offer possibility for playing with the magnetic configuration. It means that the same element can have various spin waves dynamics in dependence on the static magnetization configuration, similar to changes of the resistivity in GMR and TMR structures for electric current. The operational functionality of magnonic device or its sub-unit can be reprogrammable effectively[70–72] and used for instance to prototype magnonic transistors.[23] All these properties make magnonics and especially MCs of thin-film geometry, being a main

building block of magnonics, interesting also for a number of other fields of nanoscience and nanotechnology.[23,96,108]

VI. CONCLUDING REMARKS

Spin wave propagation in ferromagnetic materials is a complex phenomenon. The spin wave dispersion is highly anisotropic even in homogeneous thin film, where the direction of the external magnetic field with respect to the orientation of external faces of the film specifies the particular directions in the space for spin wave propagation. Also a unique feature of magnonic systems is the presence of two competitive interactions: exchange and dipole. The relative strength of these interactions varies with the extension (or contraction) of sizes of the system or its patterning. It means that spin wave spectrum does not scale, with the sizes of the system.

Magnonic crystals are periodic magnetic structures supporting propagation of spin waves. They allow to control and manipulate the spin wave propagation. Periodicity in magnonic system can be introduced in many different ways, e.g., by: i) modulation of material parameters, ii) periodic corrugation of surfaces (modulation of width or thickness), iii) periodic modulation of boundary condition on the interfaces with non magnetic medium, iv) application of periodic external magnetic field. The spin waves propagating in magnonic crystal have a form of Bloch waves. Due to the folding-back and intersection of the different branches of the dispersion relation the frequency band gaps, forbidden for spin wave propagation can be opened. By adjusting structural and material parameters of the magnonic crystal we can tune the spectrum of spin waves.

For the description of spin wave dynamics in the nm and larger scale the classical equation of motion for magnetic moment in an effective magnetic field called Landau-Lifshitz equation is commonly used. In this approach magnetic material is described not as the atomic lattice of spins but as a medium with continuous distribution of the magnetization. Also the exchange interaction, and if required other type of interactions (e.g., Dzyaloshinskii-Moriya interactions and magnetocrystalline anisotropy) are expressed as spatially continuous magnetic fields, giving the contribution to the total effective magnetic field. The modification of the dots or antidots shape, their rotations with respect to the crystallographic axis, imperfections in their shape or at their edges can further modify SW spectra. Thus, the abundance

of dots or antidots shapes, their arrangements and magnetic configurations which can be realized in MCs, makes magnonics inexhaustible and intriguing topic of research.

For technological applications of magnonics, especially in integrated devices and magnon spintronics, the MCs of thin-film geometry are expected to play a crucial role. The study of spin wave dynamics in planar magnonic films is also very interesting from scientific point of view. This is because of anisotropy of the dispersion relation of spin waves is easily modulated by external factors like magnetic field, which combines the positive and negative group velocities. Such metamaterial properties in photonics and other fields are only hardly accessible with sophisticated structuring. Magnonics allows for experimental investigation of the band structure formation in periodically structured materials with positive and negative group velocities; study a transmission and reflection of waves from negative/ positive refractive index media; consideration of the structures with sharp, graded or periodic interfaces; re-programmable band structure by changing the configuration of the static magnetization, and utilization of nonreciprocal properties in wave propagation due to permanent violation of the reciprocity principle or to study influence of nonlinearity — an inherent element of the magnetization dynamics.

Acknowledgments

This project has received funding from the European Unions Horizon 2020 research and innovation programme under the Marie Sklodowska-Curie GA No 644348 and National Science Centre of Poland project DEC-2-12/07/E/ST3/00538. The part of calculations presented in this paper were performed at the Poznan Supercomputing and Networking Center.

APPENDIX A: MATERIAL PARAMETERS

As components of MC crystals different kinds of magnetic materials can be used. The basic parameters of the selected materials used in this paper are listed in the Table I. So far, the most intensively investigated was ferrimagnetic dielectric YIG[109] and metallic Py.

TABLE I: Values of material parameters: spontaneous magnetization M_S and exchange stiffness constant A of the materials considered in this paper (see, e.g. Ref. [110]).

Material	M_S [10^6 A/m]	A [10^{-11} J/m]
Fe	1.752	1.88
Co	1.39	2.8
Py($Ni_{80}Fe_{20}$)	0.810	1.0
Ni	0.480	0.86
YIG	0.136	0.4

APPENDIX B: LIST OF ABBREVIATIONS

TABLE II: List of abbreviations used in the paper.

Abbreviation	Expansion
1D, 2D, 3D	one-, two-, three-dimensional
ADL	antidot lattice
BA	mode with the nodal lines along the direction of the external magnetic field
bcc	body-centered cubic
BMC	bi-component MCs
BVMW	backward volume magnetostatic wave geometry
BZ	Brillouin zone
DE	Damon-Eshbach geometry
ELM	empty lattice model
EM	edge mode
fcc	face-centered cubic
FDM	finite difference method
FEM	finite elements method
FFT	fast Fourier transform
FM	fundamental mode
FMR	ferromagnetic resonance
FVMW	forward volume magnetostatic wave geometry
LL	Landau-Lifshitz
MC	magnonic crystal
mFT	magnetoferritin
MS	micromagnetic simulations
NN	nearest neighbors
PSSW	perpendicular standing spin waves
PWM	plane wave method
Py	permalloy
sh	simple hexagonal
SW	spin waves
YIG	yttrium iron garnet

[1] E. Yablonovitch, Phys. Rev. Lett. **58**, 2059 (1987).

[2] S. John, Phys. Rev. Lett. **58**, 2486 (1987).

[3] J. W. Strutt, Phil. Mag. S5 **24**, 145 (1887).

[4] G. Floquet, Annales de l'École Normale Supŕieure **12**, 47 (1883).

[5] G. W. Hill, Acta Math. **8**, 1 (1886).

[6] F. Bloch, Zeitschrift fr Physik **52**, 555 (1929).

[7] F. Bloch, Z. Phys. **61**, 206 (1930).

[8] F. Bloch, Z. Phys. **74**, 295 (1932).

[9] L. Brillouin, *Wave propagation in periodic structures. Electric filters and crystal lattices* (Dover Publications, 1953), 2nd ed.

[10] P. Yeh, J. Opt. Soc. Am. **67**, 423 (1977).

[11] C. Elachi, Proceedings of the IEEE **64**, 1666 (1976).

[12] C. G. Sykes, J. D. Adam, and J. H. Collins, Appl. Phys. Lett. **29**, 388 (1976).

[13] J. P. Parekh and H. S. Tuan, Appl. Phys. Lett. **30**, 667 (1977).

[14] P. Hartemann, J. Appl. Phys. **62**, 2111 (1987).

[15] J. M. Owens, J. H. Collins, C. V. Smith, and I. I. Chiang, Appl. Phys. Lett. **31**, 781 (1977).

[16] J. Owens, J.M., C. Smith, S. Lee, and J. Collins, IEEE Trans. Magn. **14**, 820 (1978).

[17] J. O. Vasseur, L. Dobrzynski, B. Djafari-Rouhani, and H. Puszkarski, Phys. Rev. B **54**, 1043 (1996).

[18] M. Krawczyk and H. Puszkarski, Acta Physica Polonica A **93**, 805 (1998).

[19] Y. V. Gulyaev and S. A. Nikitov, Dokl. Physics **46**, 687 (2001).

[20] H. Puszkarski and M. Krawczyk, Solid State Phenomena **94**, 125 (2003).

[21] N. W. Ashcroft and N. D. Mermin, *Solid State Physics* (Philadelphia: Saunders College, 1976).

[22] J. D. Joannopoulos, S. G. Johnson, J. N. Winn, and R. D. Meade, *Photonic Crystals: Molding the flow of light* (Princeton Univ. Press., 2008), 2nd ed.

[23] M. Krawczyk and G. Grundler, J. Phys.: Condens. Matter **26**, 123202 (2014).

[24] C. Kittel, Phys. Rev. **73**, 155 (1948).

[25] A. Gurevich and G. Melkov, *Magnetization oscillations and waves* (CRC Press, Boca Raton, 1996).

[26] D. D. Stancil and A. Prabhakar, *Spin waves. Theory and applications* (Springer, 2009).

[27] L. R. Walker, Phys. Rev. **105**, 390 (1957).

[28] C. Herring and C. Kittel, Phys. Rev. **81**, 869 (1951).

[29] B. Kalinikos and A. Slavin, J. Phys. C **19**, 7013 (1986).

[30] S. Saha, R. Mandal, S. Barman, D. Kumar, B. Rana, Y. Fukuma, S. Sugimoto, Y. Otani, and A. Barman, Adv. Funct. Mater. **23**, 2378 (2013).

[31] R. Mandal, S. Saha, D. Kumar, S. Barman, S. Pal, D. Kaustuv, A. K. Raychaudhuri, Y. Fukuma, Y. Otani, and A. Barman, ACS Nano **6**, 3397 (2012).

[32] T. Schwarze and D. Grundler, Appl. Phys. Lett. **102**, 222412 (2013).

[33] R. Bali, M. Kostylev, D. Tripathy, A. O. Adeyeye, and S. Samarin, Phys. Rev. B **85**, 104414 (2012).

[34] E. K. Semenova, F. Montoncello, S. Tacchi, G. Dürr, E. Sirotkin, E. Ahmad, M. Madami, G. Gubbiotti, S. Neusser, D. Grundler, et al., Phys. Rev. B **87**, 174432 (2013).

[35] G. Gubbiotti, S. Tacchi, G. Carlotti, N. Singh, S. Goolaup, A. O. Adeyeye, and M. Kostylev, Appl. Phys. Lett. **90**, 092503 (2007).

[36] S. Tacchi, F. Montoncello, M. Madami, G. Gubbiotti, G. Carlotti, L. Giovannini, R. Zivieri, F. Nizzoli, S. Jain, A. O. Adeyeye, et al., Phys. Rev. Lett. **107**, 127204 (2011).

[37] A. I. Akhiezer, V. G. Bar'yakhtar, and S. V. Peletminskii, *Spin waves* (North Holland, Amsterdam, 1968).

[38] P. Kabos and V. S. Stalmachov, *Magnetostatic waves and their applications* (Chapman Hall and Ister Science Press, 1994).

[39] G. Bastard, *Wave Mechanics Applied to Semiconductor Heterostructures* (Les editions de Physique, Paris, 1988).

[40] C. Goffaux, V. Lousse, and J. P. Vigneron, Phys. Rev. B **62**, 7133 (2000).

[41] J. W. Klos and M. Krawczyk, J. Appl. Phys. **106**, 093703 (2009).

[42] F. Keffer, *Spin Waves* (Springer-Verlag, Berlin, 1966).

[43] S. Chikazumi, *Physics of Ferromagnetism* (Oxford University Press, 1997).

[44] M. Krawczyk, M. Sokolovskyy, J. W. Kłos, and S. Mamica, Advances in Condensed Matter Physics **2012** (2012).

[45] V. V. Kruglyak, O. Y. Gorobets, Y. I. Gorobets, and A. N. Kuchko, J. Phys.: Condens. Matter **26**, 406001 (2014).

[46] J. D. Jackson, *Classical Electrodynamics* (John Wiley and Sons, 1976), 3rd ed.

[47] J. Kaczer and L. Murtinova, phys. stat. sol. (a) **23**, 79 (1974).

[48] S. Neusser, H. G. Bauer, G. Duerr, R. Huber, S. Mamica, G. Woltersdorf, M. Krawczyk, C. H. Back, and D. Grundler, Phys. Rev. B **84**, 184411 (2011).

[49] S. Tacchi, B. Botters, M. Madami, J. W. Kłos, M. L. Sokolovskyy, M. Krawczyk, G. Gubbiotti, G. Carlotti, A. O. Adeyeye, S. Neusser, et al., Phys. Rev. B **86**, 014417 (2012).

[50] M. Krawczyk, S. Mamica, M. Mruczkiewicz, J. W. Kłos, S. Tacchi, M. Madami, G. Gubbiotti, G. Duerr, and D. Grundler, J. Phys. D: Appl. Phys. **46**, 495003 (2013).

[51] V. Kruglyak and R. Hicken, J. Magn. Magn. Mater. **2006**, 191 (2006).

[52] M. Dornik and V. Kruglyak, Phys. Rev. B **84**, 140405 (2011).

[53] S.-K. Kim, J. Phys. D: Appl. Phys. **43**, 264004 (2010).

[54] G. Venkat, D. Kumar, M. Franchin, O. Dmytriiev, M. Mruczkiewicz, H. Fangohr, A. Barman, M. Krawczyk, and A. Prabhakar, IEEE Trans. Magn. **49**, 524 (2013).

[55] M. Grimsditch, L. Giovannini, F. Montoncello, F. Nizzoli, G. K. Leaf, and H. G. Kaper, Phys. Rev. B **70**, 054409 (2004).

[56] M. Mruczkiewicz, M. Krawczyk, V. K. Sakharov, Y. V. Khivintsev, Y. A. Filimonov, and S. A. Nikitov, J. Appl. Phys. **113**, 093908 (2013).

[57] I. S. Maksymov and M. Kostylev, Physica E **69**, 253293 (2015).

[58] K.-S. Lee, D.-S. Han, and S.-K. Kim, Phys. Rev. Lett. **102**, 127202 (2009).

[59] K. Di, H. S. Lim, V. L. Zhang, M. H. Kuok, S. C. Ng, M. G. Cottam, and H. T. Nguyen, Phys. Rev. Lett. **111**, 149701 (2013).

[60] D. Kumar, J. W. Kłos, M. Krawczyk, and A. Barman, J. Appl. Phys. **115**, 043917 (2014).

[61] J. W. Klos, D. Kumar, M. Krawczyk, and A. Barman, Sci. Rep. **3**, 2444 (2013).

[62] F. Ciubotaru, A. V. Chumak, B. Obry, A. A. Serga, and B. Hillebrands, Phys. Rev. B **88**, 134406 (2013).

[63] O. Dmytriiev, V. V. Kruglyak, M. Franchin, H. Fangohr, L. Giovannini, and F. Montoncello, Phys. Rev. B **87**, 174422 (2013).

[64] J. W. Klos, K. M. Kumar, D., and A. Barman, Phys. Rev. B **89**, 014406 (2014).

[65] J. W. Klos, D. Kumar, J. Romero Vivas, H. Fangohr, M. Franchin, M. Krawczyk, and A. Barman, Phys. Rev. B **86**, 184433 (2012).

[66] Z. K. Wang, V. L. Zhang, H. S. Lim, S. C. Ng, M. H. Kuok, S. Jain, and A. O. Adeyeye, Appl.

Phys. Lett. **94**, 083112 (2009).

[67] M. Sokolovsky and M. Krawczyk, J. Nanopart. Res. **13**, 6085 (2011).

[68] C. S. Lin, H. S. Lim, Z. K. Wang, S. C. Ng, and M. H. Kuok, Appl. Phys. Lett. **98**, 022504 (2011).

[69] G. Gubbiotti, M. Kostylev, S. Tacchi, M. Madami, G. Carlotti, J. Ding, A. O. Adeyeye, F. Zighem, A. A. Stashkevich, E. Ivanov, et al., J. Phys. D: Appl. Phys. **47**, 105003 (2014).

[70] J. Topp, G. Duerr, K. Thurner, and D. Grundler, Pure Appl. Chem. **83**, 1989 (2011).

[71] R. Huber, T. Schwarze, and D. Grundler, Phys. Rev. B **88**, 100405(R) (2013).

[72] J. Ding, M. Kostylev, and A. O. Adeyeye, Appl. Phys. Lett. **100**, 073114 (2012).

[73] S. Tacchi, M. Madami, G. Gubbiotti, G. Carlotti, S. Goolaup, A. O. Adeyeye, N. Singh, and M. P. Kostylev, Phys. Rev. B **82**, 184408 (2010).

[74] D. Grundler, Nature Phys. **11**, 438 (2015).

[75] A. V. Chumak, V. S. Tiberkevich, A. D. Karenowska, A. A. Serga, J. F. Gregg, A. N. Slavin, and B. Hillebrands, Nature Commun. **1**, 141 (2010).

[76] L. Bai, M. Kohda, and J. Nitta, Appl. Phys. Lett. **98**, 72508 (201).

[77] V. D. Bessonov, M. Mruczkiewicz, R. Gieniusz, U. Guzowska, A. Maziewski, A. I. Stognij, and M. Krawczyk, Phys. Rev. B **91**, 104421 (2015).

[78] G. Gubbiotti, S. Tacchi, M. Madami, G. Carlotti, R. Zivieri, F. Montencello, F. Nizzoli, and L. Giovannini, in *Magnonics, Topics in Applied Physics* **125**, edited by D. S. O. and A. N. Slavin (Springer-Verlag Berlin Heidelberg, 2013), chap. Spin Wave Band Structure in Two-Dimensional Magnonic Crystals.

[79] S. Tacchi, P. Gruszecki, M. Madami, G. Carlotti, J. W. Klos, M. Krawczyk, A. Adeyeye, and G. Gubbiotti, Sci. Rep. **5**, 10367 (2015).

[80] G. Duerr, M. Madami, S. Neusser, S. Tacchi, G. Gubbiotti, G. Carlotti, and D. Grundler, Appl. Phys. Lett. **99**, 202502 (2011).

[81] S. Tacchi, G. Duerr, J. W. Kłos, M. Madami, S. Neusser, G. Gubbiotti, G. Carlotti, M. Krawczyk, and D. Grundler, Phys. Rev. Lett. **109**, 137202 (2012).

[82] G. Duerr, S. Tacchi, G. Gubbiotti, and D. Grundler, J. Phys. D: Appl. Phys. **47**, 325001 (2014).

[83] T. Schwarze, R. Huber, G. Duerr, and D. Grundler, Phys. Rev. B **85**, 134448 (2012).

[84] J. W. Kłos, M. Sokolovskyy, S. Mamica, and M. Krawczyk, J. Appl. Phys. **111**, 123910 (2012).

[85] S. Mamica, M. Krawczyk, and J. W. Kłos, Adv. Cond. Matt. Phys. **2012**, 1 (2012).

[86] Q. Wang, H. Zhang, X. Tang, H. Su, F. Bai, Y. Jing, and Z. Zhong, J. Phys. D: Appl. Phys. **47**, 065004 (2014).

[87] M. Krawczyk and H. Puszkarski, Phys. Rev. B **77**, 054437 (2008).

[88] M. Krawczyk and H. Puszkarski, Journal of Applied Physics **100**, 073905 (2006).

[89] M. Krawczyk, J. Klos, M. L. Sokolovskyy, and S. Mamica, Journal of Applied Physics **108**, 093909 (2010).

[90] S. Mamica, M. Krawczyk, M. L. Sokolovskyy, and J. Romero-Vivas, Phys. Rev. B **86**, 144402 (2012).

[91] M. Pauly, B. P. Pichon, P.-A. Albouz, S. Fleutot, C. Leuvrey, M. Trassin, J.-L. Gallani, and S. Begin-Colin, J. Mater. Chem. **16018**, 21 (2011).

[92] M. Kostylev, A. A. Stashkevich, Y. Roussigné, N. A. Grigoryeva, A. A. Mistonov, D. Menzel, N. A. Sapoletova, K. S. Napolskii, A. A. Eliseev, A. V. Lukashin, et al., Phys. Rev. B **86**, 184431 (2012).

[93] I. Yamashita, K. Iwahori, and S. Kumagai, Biochim. Biophys. Acta **1800**, 846 (2010).

[94] O. Kasyutich, A. Sarua, and W. Schwarzacher, J. Phys. D **41**, 134022 (2008).

[95] M. Okuda, J.-C. Eloi, S. E. W. Jones, A. Sarua, R. M. Richardson, and W. Schwarzacher, Nanotechnology **23**, 415601 (2012).

[96] V. V. Kruglyak, S. O. Demokritov, and D. Grundler, J. Phys. D: Appl. Phys. **43**, 264001 (2010).

[97] S. O. Demokritov and A. N. Slavin, eds., *Magnonics from fundamentals to applications* (Springer, 2013).

[98] B. Lenk, H. Ulrichs, F. Garbs, and M. Münzenberg, Phys. Rep. **507**, 107 (2011).

[99] A. V. Chumak, V. I. Vasyuchka, A. A. Serga, and B. Hillebrands, Nature Phys. **11**, 451 (2015).

[100] S. Cherepov, P. Khalili Amiri, J. G. Alzate, K. Wong, M. Lewis, P. Upadhyaya, J. Nath, M. Bao, A. Bur, T. Wu, et al., Appl. Phys. Lett. **104**, 082403 (2014).

[101] A. Khitun, M. Bao, and K. L. Wang, IEEE Trans. Magn. **44**, 2141 (2008).

[102] L. Dreher, M. Weiler, M. Pernpeintner, H. Huebl, R. Gross, M. S. Brandt, and S. T. B. Goennenwein, Phys. Rev. B **86**, 134415 (2012).

[103] F. Zighem, D. Faurie, S. Mercone, M. Belmeguenai, and H. Haddadi, J. Appl. Phys. **114**, 073902 (2013).

[104] A. Brataas, A. D. Kent, and H. Ohno, Nature Mat. **11**, 372 (2012).

[105] E. R. J. Edwards, H. Ulrichs, V. E. Demidov, S. O. Demokritov, and S. Urazhdin, Phys. Rev. B **86**, 134420 (2012).

[106] H. Yu, D. Duerr, R. Huber, M. Bahr, T. Schwarze, F. Brandl, and D. Grundler, Nature Commun. **4**, 2702 (2013).

[107] P. Pirro, T. Brcher, A. V. Chumak, B. Lgel, C. Dubs, O. Surzhenko, P. Grnert, B. Leven, and B. Hillebrands, Appl. Phys. Lett. **104**, 012402 (2014).

[108] S. Neusser and D. Grundler, Adv. Mater. **21**, 2927 (2009).

[109] A. A. Serga, A. V. Chumak, and B. Hillebrands, J. Phys. D: Appl. Phys. **43**, 264002 (2010).

[110] C. A. F. Vaz, J. A. C. Bland, and G. Lauhoff, Rep. Prog. Phys. **71**, 056501 (2008).

[111] J. O. Artman, Phys. Rev. **105**, 62 (1957).

[112] J. O. Artman, Phys. Rev. **105**, 74 (1957).

[113] A. Aharoni, IEEE Trans. Magn. **27**, 3539 (1991).

[114] The static effective field defines the equilibrium orientation of the magnetization and can be calculated by minimization of the self-energy, usually composed of a demagnetizing term (see Sec. III B 3) and possible anisotropy terms. Since here we focus on the spin-wave dynamics, the derivation of the equilibrium orientation of the magnetization is omitted in this paper, and the interested reader is referred to Refs. [111–113].

[115] This statement is in fact another formulation of the Bloch's theorem.

[116] Reciprocal lattice vectors are vectors which fulfill the relation $e^{i\mathbf{G}\cdot\mathbf{a}} = 1$.[21]

[117] In homogeneous film, Eq. (11) the magnetostatic potential was related only to the dynamic components of the field.